Published for SISSA by Springer

Received: December 23, 2022
Accepted: January 3, 2023
Published: January 20, 2023

Muon-electron scattering at NNLO

A. Broggio,[a] **T. Engel,**[b,c,d] **A. Ferroglia,**[e,f] **M.K. Mandal,**[g,h] **P. Mastrolia,**[i,g] **M. Rocco,**[b] **J. Ronca,**[j] **A. Signer,**[b,c] **W.J. Torres Bobadilla,**[k] **Y. Ulrich**[l] **and M. Zoller**[b]

[a] *Faculty of Physics, University of Vienna, Boltzmanngasse 5, A-1090 Vienna, Austria*

[b] *Paul Scherrer Institut, CH-5232 Villigen PSI, Switzerland*

[c] *Physik-Institut, Universität Zürich, Winterthurerstrasse 190, CH-8057 Zürich, Switzerland*

[d] *Albert-Ludwigs-Universität Freiburg, Physikalisches Institut, Hermann-Herder-Straße 3, D-79104 Freiburg, Germany*

[e] *Physics Department, New York City College of Technology, The City University of New York, 300 Jay Street, Brooklyn, NY 11201, U.S.A.*

[f] *The Graduate School and University Center, The City University of New York, 365 Fifth Avenue, New York, NY 10016, U.S.A.*

[g] *INFN, Sezione di Padova, Via Marzolo 8, I-35131 Padova, Italy*

[h] *Mani L. Bhaumik Institute for Theoretical Physics, UCLA Department of Physics and Astronomy, Los Angeles, CA 90095, U.S.A.*

[i] *Dipartimento di Fisica e Astronomia, Università degli Studi di Padova, Via Marzolo 8, I-35131 Padova, Italy*

[j] *Dipartimento di Matematica e Fisica, Università degli Studi Roma Tre and INFN, Sezione di Roma Tre, Via della Vasca Navale 84, I-00146 Roma, Italy*

[k] *Max-Planck-Institut für Physik, Werner-Heisenberg-Institut, Föhringer Ring 6, D-80805 München, Germany*

[l] *Institute for Particle Physics Phenomenology, University of Durham, South Road, Durham DH1 3LE, U.K.*

E-mail: alessandro.broggio@unimib.it, tim.engel@psi.ch, aferroglia@citytech.cuny.edu, tpmanojm@gmail.com, pierpaolo.mastrolia@pd.infn.it, marco.rocco@psi.ch, ronca.jonathan91@gmail.com, adrian.signer@psi.ch, torres@mpp.mpg.de, yannick.ulrich@durham.ac.uk, max.zoller@psi.ch

https://doi.org/10.1007/JHEP01(2023)112

JHEP01(2023)112

Abstract: We present the first calculation of the complete set of NNLO QED corrections for muon-electron scattering. This includes leptonic, non-perturbative hadronic, and photonic contributions. All fermionic corrections as well as the photonic subset that only corrects the electron or the muon line are included with full mass dependence. The genuine four-point two-loop topologies are computed as an expansion in the small electron mass, taking into account both, logarithmically enhanced as well as constant mass effects using massification. A fast and stable implementation of the numerically delicate real-virtual contribution is achieved by combining OpenLoops with next-to-soft stabilisation. All matrix elements are implemented in the McMule framework, which allows for the fully-differential calculation of any infrared-safe observable. This calculation is to be viewed in the context of the MUonE experiment requiring a background prediction at the level of 10 ppm. Our results thus represent a major milestone towards this ambitious precision goal.

Keywords: Higher-Order Perturbative Calculations, Precision QED, Automation

ArXiv ePrint: 2212.06481

JHEP01(2023)112

Contents

JHEP01(2023)112

1 Introduction

The MUonE experiment [1–3] aims to measure the differential cross section for muon-electron elastic scattering by colliding a 160 GeV muon beam with atomic electrons located on thin target plates. The purpose is to derive very precisely the running of the electromagnetic coupling α at low energy using the method proposed in [4].

The need for such a measurement arises from the long-standing tension between the measured and calculated values of the anomalous magnetic moment of the muon, $a_\mu = (g-2)/2$. The discrepancy between a_μ calculated in the Standard Model (SM) and the corresponding experimental measurement was first reported by the BNL E821 experiment [5] and recently confirmed by the first results from the FNAL $g-2$ experiment [6]. The deviation between the combination of the BNL and FNAL experiments, and the currently accepted SM prediction [7] is of 4.2σ.

It is important to rule out the possibility that the deviation is due to a systematic error in the calculation. The contribution from the hadronic vacuum polarisation (HVP), a_μ^{HVP},

enters in the SM prediction and cannot be calculated in perturbation theory. Consequently, this quantity is usually determined from low-energy electron-positron annihilation data through a dispersive approach [8, 9]. Interestingly, a recent calculation in lattice QCD [10] leads to a value that is in contrast with the data-driven calculation and reduces the discrepancy between theory and experiment in the muon magnetic moment. In light of this situation, it is crucial to pursue new and different methods to determine the HVP contribution.

The method proposed in [4, 11] allows for the determination of a_μ^{HVP} from the measurement of the running electromagnetic coupling in the space-like region, which can be carried out by the MUonE experiment. Contrary to the conventional time-like approach, the space-like region has the advantage of being smooth and free of hadronic resonances. The experiment suffers, however, from complications related to the measurement of a subleading effect. The contribution of the HVP changes the differential cross section by only up to $\mathcal{O}(10^{-3})$. As a consequence, the experimental and theoretical uncertainties should not exceed 10 ppm in order to allow for a competitive determination of a_μ^{HVP}.

The feasibility of this ambitious precision goal crucially relies on two special features of muon-electron scattering at the proposed energy scale. First, the presence of a low-signal normalisation region allows for the cancellation of experimental systematic uncertainties. Second, non-perturbative hadronic corrections other than HVP only enter beyond next-to-next-to-leading order (NNLO) and can safely be neglected. This includes the notoriously difficult hadronic light-by-light scattering contribution. The NNLO HVP corrections, on the other hand, are significantly simpler and have been computed in [12] with a dispersive approach. To avoid any dependence on time-like data the analogous calculation has been performed with the space-like hyperspherical method in [13].

To ensure a clean extraction of the HVP with MUonE, it is further important to rule out any possible contamination of the signal due to physics beyond the SM (BSM). Dedicated studies performed in [14, 15] have shown that such effects could only affect the signal below 10 ppm, if existing BSM bounds are to be observed. In these analyses the normalisation region was used to cancel larger effects. This explains the different conclusion reached in [16], where the normalisation region was not exploited. Even though this latter study is therefore not directly applicable to the HVP measurement, it opens up the avenue for dedicated BSM searches with MUonE. This option was further investigated in [17–19] where it was shown that new parameter space for light new physics could indeed be explored.

At present, the main concern on the theoretical side is the perturbative prediction of the SM background at the level of 10 ppm. It is therefore mandatory to incorporate NNLO corrections in QED. In addition, it will be necessary to improve the precision of the calculation by supplementing it with large logarithmic corrections of soft and collinear origin beyond NNLO. In order to reach this goal, there has been a coordinated theoretical effort [20] with the goal of developing two completely independent Monte Carlo event generators.

The MESMER [21] Monte Carlo is based on photon-mass regularisation combined with a slicing approach to cope with soft divergences in the phase-space integration. The complete set of electroweak corrections are implemented at next-to-leading order (NLO) accuracy [22]. At NNLO, virtual as well as real leptonic contributions have been included in the form of leptonic vacuum polarisation and lepton pair production [23]. In addition, vir-

JHEP01(2023)112

tual hadronic contributions have been included through the time-like approach. However, NNLO photonic corrections have been calculated in [21] employing a YFS-inspired [24] approximation when dealing with the genuine two-loop four-point topologies. Otherwise, the contributions that only correct the electron or muon line are calculated without any approximation. Most recently, also the background due to pion production was studied with MESMER in [25].

The second Monte Carlo is being developed within the MCMULE framework [26] and it is employed in the present paper. It is based on dimensional regularisation and the FKS$^\ell$ subtraction scheme [27], a generalisation of the FKS method [28, 29] for QED with massive fermions to any order in perturbation theory. The subset of NNLO QED corrections restricted to the electron line has been implemented in [26]. Perfect agreement was found in a dedicated comparison with the MESMER code. In the following, we present the calculation of the full set of NNLO QED corrections in MCMULE.

Contrary to QCD experiments, MUonE observables are not collinear safe and therefore highly sensitive to fermion-mass effects. It is therefore not permissible to neglect the electron mass, even though it is small compared to all other scales in the process. This has far-reaching ramifications. On the one hand, it simplifies the infrared (IR) structure since collinear singularities are naturally regularised by fermion masses. At the same time, it significantly complicates the evaluation of loop integrals. In the case of closed fermion loops this is unproblematic, since semi-numerical methods can easily be applied. In particular, we have implemented the aforementioned hyperspherical results from [13] to calculate leptonic and non-perturbative hadronic NNLO corrections. In the case of the photonic two-loop amplitude, on the other hand, the complete calculation with full mass dependence is still not available.

Very recently, however, the analytic evaluation of the amplitude of di-muon production via massless electron-positron annihilation in QED [30], as well as the heavy-quark pair production through light-quark annihilation in QCD [31], became available, based on the master integrals computed in [31–33]. These two results have shown the feasibility of a completely analytical calculation of the NNLO virtual muon-electron elastic scattering in the approximation of a massless electron, presented here for the first time. This result can be employed in the context of the MUonE observables if supplemented with finite electron-mass effects introduced via massification, which was originally developed in [34–36] and later extended to heavy external states in [37]. It exploits the universal structure of collinear degrees of freedom to determine the leading mass effects in a process-independent way. This includes the logarithmically enhanced as well as the constant terms and only neglects polynomially suppressed contributions. Since the electron mass is much smaller than all other scales in the process, this procedure is expected to yield a reliable approximation of the full mass dependence.

At the same time, this scale hierarchy gives rise to numerical instabilities in the case of soft and collinear photon emission. Following [38] we apply next-to-soft (NTS) stabilisation combined with OPENLOOPS [39, 40] to ensure a fast and stable implementation of the delicate real-virtual amplitude. This method is based on the idea of expanding the real-virtual contribution in the soft photon energy including the next-to-leading power term

JHEP01(2023)112

in numerically delicate phase-space corners. Similar to the eikonal contribution at leading power, also the subleading term can be related to the non-radiative process. This was shown in [41] where the Low-Burnett-Kroll theorem [42, 43] was extended to the one-loop level.

The paper is structured as follows. Section 2 presents the technical details of the calculation. This includes a discussion of the one-loop radiative and the two-loop amplitude, as well as details on the implementation in the McMule framework. Section 3 presents results for observables that are relevant for the MUonE experiment. The calculation has been validated with various tests, including, among others, a dedicated study for the reliability of the massified approximation as well as for the NTS stabilisation, which are discussed in section 4. We conclude and remark on future steps in section 5.

2 Technical details

The complete NNLO results for muon-electron scattering presented in this article represent the culmination of a program involving various groups over several years. They are based on numerous concepts and calculations that have been developed for this program and were published in separate articles. In this section, we will build on these articles, give an overview of how the partial results are combined and describe what additional steps were required. In the interest of conciseness, we will refrain from repeating the details of previous work that is required to obtain the physical results presented here. Instead, we will refer the reader at the appropriate places to those earlier papers for further details.

2.1 Overview

The fully differential computation of elastic muon-electron scattering at higher orders in α follows closely the procedure outlined in [20] whose notation we also adopt. To obtain results at NNLO we need to consider the processes with up to two additional photons,

$$e^-(p_1)\,\mu^\pm(p_2) \to e^-(p_3)\,\mu^\pm(p_4) + \{\gamma(k_1)\,\gamma(k_2)\}\,. \tag{2.1}$$

Lepton pair production, i.e. $e^-\mu^\pm \to e^-\mu^\pm(e^+e^-)$, will not be considered here. Even though this process plays an important role in a future MUonE analysis, it is a measurably different physical process and from a theoretical point of view can be considered in isolation [23]. As discussed in [20], the trivial inclusion of the tree-level Z exchange is needed to match the precision required by MUonE, but the full NLO electroweak effects are below the 10 ppm target precision as shown in a calculation by Mesmer [22]. We have implemented the same corrections in McMule in the context of $ee \to \mu\mu$ [44] and found full agreement. Nevertheless, these corrections are not considered in this paper where we restrict ourselves to pure QED.

We will denote the ℓ-loop amplitude of the process (2.1) with j additional photons by $\mathcal{A}^{(\ell)}_{n+j}$. The (differential) LO cross section $\mathrm{d}\sigma_0$ is obtained by integrating the tree-level (squared) matrix element for the $2 \to 2$ process $\mathcal{M}^{(0)}_n \equiv |\mathcal{A}^{(0)}_n|^2$ over the two-particle phase space $\mathrm{d}\Phi_n$.

In addition to the flux factor, a measurement function $O(p_3, p_4, \{k_1, k_2\})$ that defines the observable is implicitly understood to be part of the phase-space integration. The only

JHEP01(2023)112

constraint on this function is that it represents an IR-safe quantity. This property is crucial to ensure the cancellation of IR singularities when going beyond LO. Concretely, in the soft limit of e.g. $k_1 \to 0$ we require $O(p_3, p_4, k_1, \{k_2\}) \to O(p_3, p_4, \{k_2\})$. Contrary to computations in QCD, there is no requirement on O for a collinear limit $k_i \| p_j$. The potential non-cancellation of contributions from collinear regions of the phase space is regularised by the fermion masses. The corresponding logarithms are physical. They can be and are measured. As a consequence, in order to be fully differential, in particular with respect to emission of collinear photons, muon mass M and electron mass m effects have to be included.

As we will discuss below, our calculation includes full dependence on M, but makes certain approximations regarding the m dependence. These approximations are restricted to the (finite part of the) two-loop matrix elements $\mathcal{M}_n^{(2)}$, as given in (2.4), and are driven by the complexity of two-loop calculations with many scales. Even with these approximations, there are no collinear singularities present and only soft singularities appear. This leads to a tremendous simplification of the IR structure and allows the use of the FKS^2 subtraction method [27] to perform a fully differential phase-space integration also at NNLO.

Radiative corrections to muon-electron scattering have been considered in the past [45–51], using various approximations. Two independent fully differential results with complete muon and electron mass dependence exist and have been compared [22, 26]. As is well known, the NLO correction to the (differential) cross section $\mathrm{d}\sigma^{(1)}$ is a combination of real and virtual contributions

$$\mathrm{d}\sigma^{(1)} = \mathrm{d}\sigma^{(\mathrm{v})} + \mathrm{d}\sigma^{(\mathrm{r})} = \int \mathrm{d}\Phi_n \, \mathcal{M}_n^{(1)} + \int \mathrm{d}\Phi_{n+1} \, \mathcal{M}_{n+1}^{(0)} \,, \tag{2.2}$$

where $\mathcal{M}_n^{(1)} = 2\,\mathrm{Re}[\mathcal{A}_n^{(1)} \times (\mathcal{A}_n^{(0)})^*]$ and $\mathcal{M}_{n+1}^{(0)} = |\mathcal{A}_{n+1}^{(0)}|^2$. For an IR-safe observable, the IR singularities cancel between $\mathrm{d}\sigma^{(\mathrm{v})}$ and $\mathrm{d}\sigma^{(\mathrm{r})}$. We do the renormalisation in terms of on-shell fermion masses and the on-shell coupling $\alpha \equiv \alpha(0)$. Intermediate results depend on the regularisation scheme, but this scheme dependence cancels for physical predictions. In McMule the standard choice is to use the four-dimensional helicity scheme (FDH) [52].

The NNLO corrections to the cross section are obtained as the sum of three contributions, dubbed double-virtual (vv), real-virtual (rv), double-real (rr) terms, as

$$\mathrm{d}\sigma^{(2)} = \mathrm{d}\sigma^{(\mathrm{vv})} + \mathrm{d}\sigma^{(\mathrm{rv})} + \mathrm{d}\sigma^{(\mathrm{rr})} = \int \mathrm{d}\Phi_n \, \mathcal{M}_n^{(2)} + \int \mathrm{d}\Phi_{n+1} \, \mathcal{M}_{n+1}^{(1)} + \int \mathrm{d}\Phi_{n+2} \, \mathcal{M}_{n+2}^{(0)} \,, \tag{2.3}$$

where the matrix elements are defined as

$$\mathcal{M}_n^{(2)} = 2\,\mathrm{Re}\Big[\mathcal{A}_n^{(2)} \times (\mathcal{A}_n^{(0)})^*\Big] + \big|\mathcal{A}_n^{(1)}\big|^2 \equiv \mathcal{M}_n^{(2+0)} + \mathcal{M}_n^{(1+1)} \,, \tag{2.4}$$

$$\mathcal{M}_{n+1}^{(1)} = 2\,\mathrm{Re}\big[\mathcal{A}_{n+1}^{(1)} \times (\mathcal{A}_{n+1}^{(0)})^*\big] \,, \tag{2.5}$$

$$\mathcal{M}_{n+2}^{(0)} = \big|\mathcal{A}_{n+2}^{(0)}\big|^2 \,. \tag{2.6}$$

Taken separately, the three parts of (2.3) are IR divergent. Following the FKS^2 procedure [27], we re-express the NNLO corrections as a sum of three separately finite parts

$$\mathrm{d}\sigma^{(2)} = \mathrm{d}\sigma_n^{(2)}(\xi_c) + \mathrm{d}\sigma_{n+1}^{(2)}(\xi_c) + \mathrm{d}\sigma_{n+2}^{(2)}(\xi_c) \,. \tag{2.7}$$

JHEP01(2023)112

According to (2.7), $\mathrm{d}\sigma^{(2)}$ consists of a two-particle part $\mathrm{d}\sigma_n^{(2)}(\xi_c)$ that combines the double virtual with suitable integrated real corrections to obtain an IR finite result, a three-particle part $\mathrm{d}\sigma_{n+1}^{(2)}(\xi_c)$ related to real-virtual corrections, and a four-particle part $\mathrm{d}\sigma_{n+2}^{(2)}(\xi_c)$ that corresponds to soft-subtracted double-real corrections. These parts individually depend on an unphysical parameter ξ_c. As will be illustrated in section 4.2.1, this ξ_c dependence has to cancel in the sum, providing a very useful check of a correct and numerically stable implementation.

The higher-order corrections to the cross section can be split into photonic and fermionic corrections. The latter contain leptonic vacuum polarisation (VP) contributions, $\mathrm{d}\sigma_{\mathrm{lep}}^{(i)}$, and are separately gauge independent. We include electron, muon, and tau loops in our results with all mass effects. In addition we also provide results for hadronic loops, $\mathrm{d}\sigma_{\mathrm{had}}^{(i)}$, i.e. the signal of the MUonE experiment. The photonic corrections can be split further into separately gauge independent pieces by formally differentiating between the electron charge q and the muon charge Q, and organising the matrix elements according to powers of q and Q. The tree-level matrix element of the $2 \to 2$ process has couplings $\mathcal{M}_n^{(0)} \sim q^2\,Q^2$. At NLO, there are contributions with an additional factor q^2 (electronic corrections $\mathrm{d}\sigma_e^{(1)}$), an additional factor Q^2 (muonic corrections $\mathrm{d}\sigma_\mu^{(1)}$), and an additional factor $q\,Q$ (mixed corrections $\mathrm{d}\sigma_{e\mu}^{(1)}$). In analogy to lepton-proton scattering, the latter are known as two-photon exchange contributions. With respect to the Born contribution, at NNLO there are four additional factors of q or Q for the photonic corrections. Following the NLO terminology, we will consider a split into electronic ($\mathrm{d}\sigma_e^{(2)}$, additional factor q^4), muonic ($\mathrm{d}\sigma_\mu^{(2)}$, additional factor Q^4) and various mixed corrections with additional factors (q^3Q, q^2Q^2, qQ^3). The latter are often combined into $\mathrm{d}\sigma_{e\mu}^{(2)}$ for the presentation of the results, even though they are computed separately. Hence, at NLO ($\ell = 1$) and NNLO ($\ell = 2$), we decompose (2.2) and (2.3) as

$$\mathrm{d}\sigma^{(\ell)} = \mathrm{d}\sigma_e^{(\ell)} + \mathrm{d}\sigma_{e\mu}^{(\ell)} + \mathrm{d}\sigma_\mu^{(\ell)} + \mathrm{d}\sigma_{\mathrm{lep}}^{(\ell)} + \mathrm{d}\sigma_{\mathrm{had}}^{(\ell)}\,. \tag{2.8}$$

Some (squared) matrix elements contributing to $\mathrm{d}\sigma^{(2)}$ are depicted in figure 1. An example for the fermionic corrections $\mathrm{d}\sigma_{\mathrm{lep}}^{(\ell)}$ and $\mathrm{d}\sigma_{\mathrm{had}}^{(\ell)}$ is shown in the top left panel of figure 1. The vv cuts correspond to $\mathcal{M}_n^{(2)}$, the first due to the one-loop amplitude squared $\mathcal{M}_n^{(1+1)}$, the second due to the interference of the two-loop amplitude with the tree-level amplitude $\mathcal{M}_n^{(2+0)}$. The rv cut corresponds to a $\mathcal{M}_{n+1}^{(1)}$ contribution. For photonic corrections we also have rr cuts, due to double real contributions involving $\mathcal{M}_{n+2}^{(0)}$. Contributions to $\mathrm{d}\sigma_e^{(2)}$ and $\mathrm{d}\sigma_\mu^{(2)}$ are also shown in the top panel of figure 1, whereas the bottom panel depicts various contributions to $\mathrm{d}\sigma_{e\mu}^{(2)}$.

The split (2.8) has a threefold motivation. First, since the electron mass is much smaller than the muon mass, the electronic corrections are expected to be numerically more important. As we will see, however, this expectation is only partially correct. Second, the electronic and muonic corrections can be computed with full dependence on the electron mass m as well as the muon mass M [21, 26], since the two-loop amplitudes can be expressed through the massive two-loop form factor [53–55]. We use a solid single line for the electron in figure 1 to indicate that all m effects are fully taken into account. As we will see below,

JHEP01(2023)112

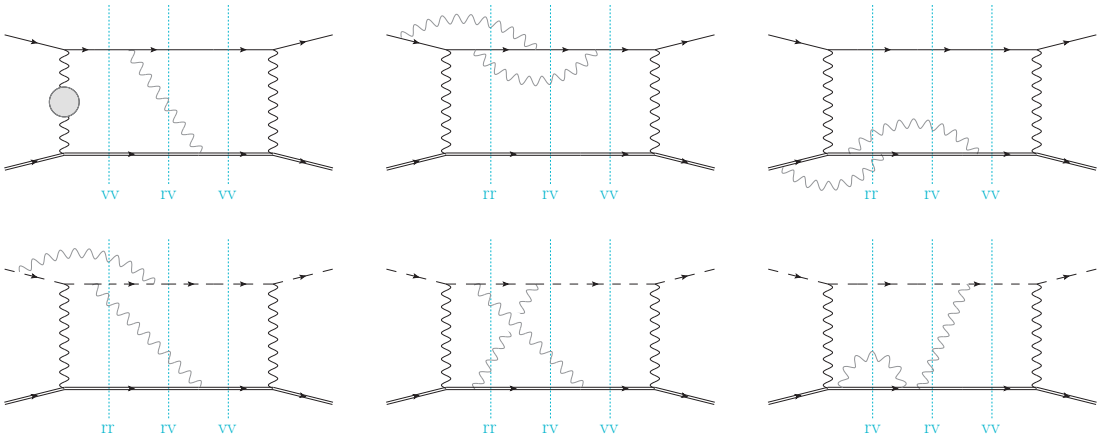

Figure 1. Sample contributions to the (squared) matrix elements $\mathcal{M}_n^{(2)}$ (vv), $\mathcal{M}_{n+1}^{(1)}$ (rv), and $\mathcal{M}_{n+2}^{(0)}$ (rr). The leading order part $\mathcal{M}_n^{(0)} \sim q^2\,Q^2$ is shown in black while additional particles are shown in grey. The top-left panel shows fermionic corrections. Electronic (muonic) corrections are shown in the top-middle (right) panel, with all additional emissions $\sim q^4$ ($\sim Q^4$) from the electron (muon) line. Muon mass effects (solid double line) and electron mass effects (single solid line) are taken into account exactly. The bottom panel shows examples of mixed corrections, with additional couplings $q^3\,Q$ (left panel), $q^2\,Q^2$ (middle panel), and $q\,Q^3$ (right panel). For these contributions electron mass effects in $\mathcal{M}_n^{(2)}$ (vv) are included only through massification (see text), as indicated by the dashed single line.

for the mixed corrections shown in the bottom panel of figure 1, electron mass effects in the two-loop matrix element are taken into account approximately, as indicated by using a dashed single line for the electron. Finally, changing from μ^+ to μ^- simply amounts to the replacement $Q \to -Q$. In particular, the electronic and muonic corrections are not affected.

Once the amplitudes for muon-electron scattering are known, we can follow the procedure used previously for Bhabha scattering [38], Møller scattering [56], and lepton pair production [44] to obtain physical results. The double radiative tree-level matrix element $\mathcal{M}_{n+2}^{(0)}$ is trivial to compute with full M and m dependence. The only delicate point is to ensure a numerically reliable integration over those phase-space regions that lead to collinear pseudo-singularities. This is achieved by a partitioning and tuning of the phase space to have a direct match of the small angle with an integration variable [57]. As mentioned above, the check of the independence on ξ_c of the final result plays an important role here. The remaining matrix elements, $\mathcal{M}_{n+1}^{(1)}$ and $\mathcal{M}_n^{(2)}$, are more delicate and will be discussed below, in sections 2.2 and 2.3.

2.2 One-loop radiative matrix element

The real-virtual matrix element (2.5) is particularly delicate with respect to its numerical stability. For the bulk of the phase space this contribution was computed with OpenLoops [39, 40], which recursively constructs amplitudes from process-independent building blocks given by the Feynman rules of the model. Recently, OpenLoops was extended to allow for the separate calculation of QCD, QED and weak corrections with variable number

JHEP01(2023)112

of leptons and quarks, as well as with massive leptons. In order to comply with the split of the photonic corrections discussed above, we separated the purely muonic, purely electronic and mixed corrections through a power counting in the muon and electron charges Q and q.

The OpenLoops program provides high numerical stability in one-loop amplitudes due to the on-the-fly reduction of tensor integrals[1] [39], dedicated kinematic expansions, and a hybrid precision mode [40]. In the latter, the majority of the OpenLoops recursion steps is performed in double precision, while only the most critical steps of the on-the-fly algorithm are performed in quadruple precision. While this procedure provides excellent CPU efficiency and numerical stability for a wide range of processes, even in ultra-soft and collinear regions [40], for simultaneously extremely soft and collinear kinematics the numerical stability in the hybrid precision configuration was not sufficient for this process. Hence a next-to-soft (NTS) stabilisation was employed.

The basic idea of NTS stabilisation [38] is to replace the full one-loop matrix elements by a numerically adequate expression in the critical soft regions of phase space. The well-known soft limit, given by an eikonal factor times a reduced matrix element, is not sufficiently accurate. To improve the situation, the NTS limit has to be used. This limit can be obtained by a generalisation of the Low-Burnett-Kroll theorem [42, 43] to one loop. In [41] it was shown how to write the NTS limit for one-loop matrix elements in a process independent way. With these expressions we can obtain a numerically reliable evaluation of the one-loop contribution in all regions of phase space. As will be discussed in section 4.2.3, this implementation was successfully checked against a full quadruple-precision calculation in OpenLoops.

While NTS stabilisation is crucial for the mixed real-virtual corrections, it is not strictly necessary in the case of the electronic and muonic contributions. For the results presented in [26], we have used an in-house calculation of the real- virtual contribution assisted by Collier [58] in problematic regions of the phase space. However, this implementation is superseded in the current version of the code by OpenLoops combined with NTS stabilisation. Even though this results in a slower evaluation speed for the matrix element, the improved numerical stability ensures a faster and more reliable phase-space integration.

2.3 Double-virtual matrix element

As a final ingredient for the NNLO corrections, we need the double-virtual matrix element $\mathcal{M}_n^{(2)}$.

Following [13], the fermionic contributions at two loop, $\mathrm{d}\sigma_{\mathrm{lep}}^{(2)}$ and $\mathrm{d}\sigma_{\mathrm{had}}^{(2)}$, can be calculated with full M and m dependence, using the hyperspherical method [60–62]. This semi-numerical approach is independent of the exact form of the VP. This therefore makes it possible to compute leptonic as well as non-perturbative hadronic contributions simultaneously. In the case of the leptonic VP the analytic two-loop result from [63] can be used. For the HVP, on the other hand, we can rely on the Fortran library `alphaQED` [64].

[1] The remaining scalar two-, three- and four-point integrals are evaluated with the external tools Collier [58] (double precision calculation) or OneLoop [59] (quadruple precision).

JHEP01(2023)112

For the photonic part of $\mathcal{M}_n^{(2)}$, according to (2.4), we need $\mathcal{A}_n^{(1)}$ and $\mathcal{A}_n^{(2)}$, decomposed as

$$\mathcal{A}_n^{(1)} = q^3 Q\, \mathcal{A}_{3,1}^{(1)} + q^2 Q^2\, \mathcal{A}_{2,2}^{(1)} + q Q^3\, \mathcal{A}_{1,3}^{(1)}\,, \tag{2.9}$$

$$\mathcal{A}_n^{(2)} = q^5 Q\, \mathcal{A}_{5,1}^{(2)} + q^4 Q^2\, \mathcal{A}_{4,2}^{(2)} + q^3 Q^3\, \mathcal{A}_{3,3}^{(2)} + q^2 Q^4\, \mathcal{A}_{2,4}^{(2)} + q Q^5\, \mathcal{A}_{1,5}^{(2)}\,. \tag{2.10}$$

The purely electronic and muonic two-loop corrections, $\mathcal{A}_{5,1}^{(2)}$ and $\mathcal{A}_{1,5}^{(2)}$, with complete mass dependence, can be calculated using the known analytic results of the massive form factors [53–55]. Therefore, the terms $\mathrm{d}\sigma_e^{(2)}$ and $\mathrm{d}\sigma_\mu^{(2)}$, having complete dependence on the muon and electron mass, can be computed within the McMule framework, as previously employed in [21, 26]. On the other hand, $\mathrm{d}\sigma_{e\mu}^{(2)}$ receives contributions from the remaining photonic mixed terms, $\mathcal{A}_{4,2}^{(2)}$, $\mathcal{A}_{3,3}^{(2)}$, and $\mathcal{A}_{2,4}^{(2)}$, whose expressions with full mass dependence are currently not available. However, the electron mass m is sufficiently small with respect to all other scales S in the process to approximate $\mathrm{d}\sigma_{e\mu}^{(2)}$ by neglecting terms that are polynomially suppressed in m^2/S. As explained in detail in section 2.3.5, this expansion can be efficiently computed based on the massless result using massification.

In the following, we provide the details of the evaluation of the two terms contributing to $\mathcal{M}_n^{(2)}$ in (2.4), namely the interference term, $\mathcal{M}_n^{(2+0)} \equiv 2\,\mathrm{Re}\big[\mathcal{A}_n^{(2)} \times (\mathcal{A}_n^{(0)})^*\big]$, that receives contributions from two-loop graphs, and the contribution due to squared one-loop graphs, $\mathcal{M}_n^{(1+1)} \equiv |\mathcal{A}_n^{(1)}|^2$.

2.3.1 Two-loop contribution

The analytic evaluation of $\mathcal{M}_n^{(2+0)}(m=0)$ is carried out by considering the electron as a massless particle, while retaining full dependence on the muon mass M, and it constitutes one of the main novel results of this paper.

By adopting the same strategy as used for the crossing-related process $e^+e^- \to \mu^+\mu^-$ in [30], $\mathcal{A}_n^{(2)}(m=0)$ has been generated by FeynArts [65] and FeynCalc [66], within conventional dimensional regularisation (CDR). The decomposition of $\mathcal{M}_n^{(2+0)}$ has been carried out by the in-house calculation framework AIDA [67], that combines the Adaptive Integrand Decomposition [68, 69], and the integration-by-parts decomposition, through the interfaces to Reduze [70] libraries. The master integrals for the muon-electron elastic scattering were computed analytically in [31–33] by means of the method of differential equations [71–75] and the Magnus exponential [76, 77].

The analytic expression is obtained in the non-physical region $s<0$, $t<0$, and cast as a Laurent series expansion around $d=4$ space-time dimensions, whose coefficients are a combination of generalised polylogarithms (GPLs) [78, 79], depending on the kinematic variables. The numerical values of the amplitude in the physical region of the elastic scattering, $s>M^2$ and $-(s-M^2)^2/s<t<0$, can be obtained by evaluating the GPLs according to the prescription $s \to s+i\delta$, namely by assigning a small positive imaginary part $\delta \ll 1$.

Let us remark that the result for the amplitude of muon-electron elastic scattering is found to obey the crossing symmetry linking it to di-muon production in electron-positron fusion [30]. Moreover, the diagrams considered in the current process have been recently used also to derive the analytic expressions of the colour-stripped partial amplitudes of

JHEP01(2023)112

$q\bar{q} \to t\bar{t}$ in QCD [31], proportional to the colour coefficients corresponding to Abelian-like diagrams, and were found in agreement with the previously known results [80–82]. The matrix element has been computed in CDR, and it is expressed in terms of the on-shell muon mass and the QED coupling renormalised in the $\overline{\text{MS}}$ scheme [30].

In view of the electron massification procedure, discussed in section 2.3.5, the fermionic terms coming from diagrams with closed fermion loops, as well as the terms proportional to $q^6\,Q^2$ (purely electronic corrections) and $q^2\,Q^6$ (purely muonic corrections), are excluded from $\mathcal{M}_n^{(2+0)}(m=0)$, see (2.10), and replaced by their complete massive version.

2.3.2 Squared one-loop contribution

The determination of $\mathcal{M}_n^{(1+1)}(m=0)$ requires the knowledge of the squared one-loop amplitude $\mathcal{A}_n^{(1)}(m=0)$ up to $\mathcal{O}(\epsilon^2)$. We have performed two independent analytic calculations of the squared one-loop contribution: one using FeynArts [65] and FeynCalc [66] in CDR, and one using QGraf [83], Package-X [84], and its companion tool PVReduce in FDH. In both cases, the intermediate expressions contain only one-loop scalar integrals that, upon integration-by-parts reduction, are decomposed in terms of master integrals. The latter have been evaluated using the same technique as the two-loop integrals mentioned earlier, i.e. via the method of differential equations [71–75] and the Magnus exponential [76, 77]. Because of products of master integrals containing $1/\epsilon^2$ poles, we had to extend up to $\mathcal{O}(\epsilon^2)$ the one-loop integrals given in [32]. The complete expression of the squared one-loop contribution is finally split into electronic, muonic and photonic corrections, according to section 2.1. As for $\mathcal{M}_n^{(2+0)}(m=0)$, we also replace the terms q^2Q^6 and q^6Q^2 in $\mathcal{M}_n^{(1+1)}(m=0)$ by the analogous expression with full m dependence.

2.3.3 Infrared structure

As an additional check of $\mathcal{M}_n^{(2)}(m=0)$, we have verified that it has the expected IR structure. The residual IR poles present in the two-loop corrections evaluated at $m=0$ can be obtained by adapting a procedure originally developed for the IR structure of QCD amplitudes in [85–87]. The IR poles are dictated by an anomalous dimension Γ. The explicit expressions for the perturbative coefficients of Γ in CDR for the process $e^+\,e^- \to \mu^+\,\mu^-$ up to α^2 can be found in the supplemental material of [30]. For our process we have to use the crossed expressions with $s \leftrightarrow t$. Through the perturbative coefficients of Γ and the QED beta function, an IR renormalisation factor $Z_{\text{IR}} = 1 + Z_{\text{IR}}^{(1)} + Z_{\text{IR}}^{(2)} + \mathcal{O}(\alpha^3)$ can be written. The IR poles remaining in the UV-renormalised virtual corrections to muon-electron scattering at ℓ loops can then be obtained by multiplying Z_{IR} by the amplitude up to $(\ell-1)$ loops and subsequently collecting the terms proportional to order α^ℓ in the product. In particular, at two loops one finds

$$\begin{aligned}\mathcal{M}_n^{(2)}\Big|_{\text{poles}} = &\left[2\left(Z_{\text{IR}}^{(2)} - \left(Z_{\text{IR}}^{(1)}\right)^2\right)\mathcal{M}_n^{(0)} + Z_{\text{IR}}^{(1)}\mathcal{M}_n^{(1)}\right]_{\text{poles}} \\ &+ \left[Z_{\text{IR}}^{(1)}\mathcal{M}_n^{(1)} - \left(Z_{\text{IR}}^{(1)}\right)^2\mathcal{M}_n^{(0)}\right]_{\text{poles}} .\end{aligned} \tag{2.11}$$

In (2.11) only the IR poles in the dimensional regulator have to be retained in both the l.h.s. and r.h.s. of the equations. The first line of (2.11) leads to the IR poles of the

JHEP01(2023)112

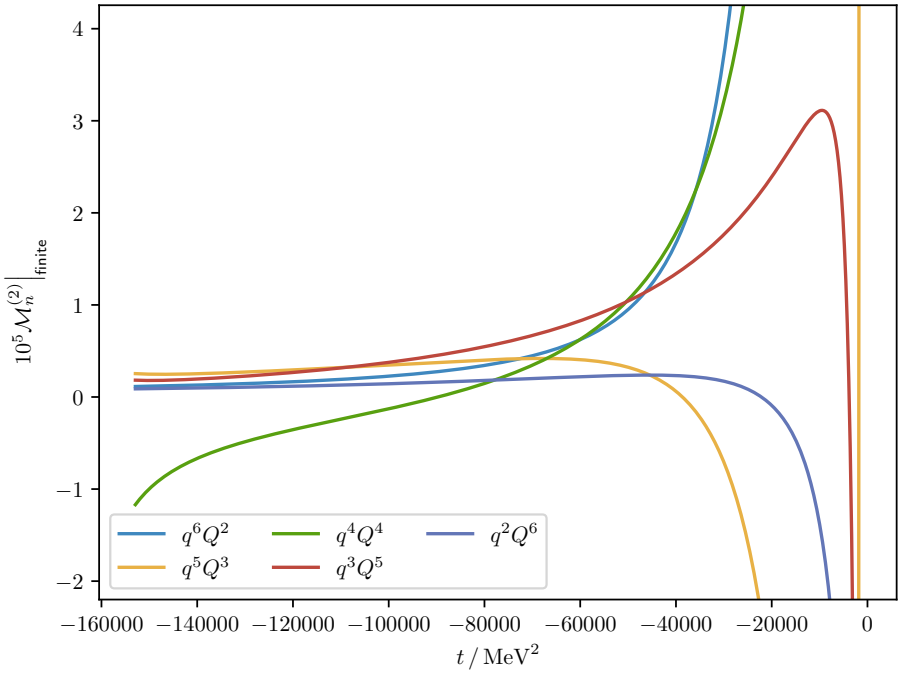

Figure 2. The finite part of the matrix element $\mathcal{M}_n^{(2)}(m=0)$, defined in (2.4), calculated in the FDH scheme, within the kinematic region used in section 3, i.e. $s = 174\,684\,\text{MeV}^2$ and $t \in [-153\,069, -1\,021]\,\text{MeV}^2$.

interference of the two-loop and tree-level amplitudes $\mathcal{M}_n^{(2+0)}(m=0)$, while the second accounts for the IR poles originating from the absolute square of the one-loop amplitude $\mathcal{M}_n^{(1+1)}(m=0)$.

2.3.4 Scheme conversion

The massless two-loop amplitude as discussed so far, has been evaluated in terms of the QED coupling renormalised in the $\overline{\text{MS}}$ scheme, whereas for the final results we use the on-shell α. Thus, in principle we have to perform a renormalisation-scheme conversion for $\mathcal{M}_n^{(2)}$. However, the difference between the two renormalisation schemes is restricted to fermion loop contributions. As discussed above, the latter are computed independently and directly in the on-shell scheme. Hence, for the photonic terms, no further shift is required.

Another scheme conversion that is needed is a regularisation-scheme change. Following the standard convention of McMule, the matrix elements are converted from the CDR scheme to the FDH scheme. This can be done by realising that the IR-subtracted matrix element is independent of the regularisation scheme [88, 89], i.e.

$$\left(Z_{\text{IR}}^{\text{FDH}}\right)^{-1}\mathcal{M}_n^{(\text{FDH})} = \left(Z_{\text{IR}}^{\text{CDR}}\right)^{-1}\mathcal{M}_n^{(\text{CDR})} + \mathcal{O}(\epsilon)\,. \tag{2.12}$$

JHEP01(2023)112

The difference between $Z_{\text{IR}}^{\text{CDR}}$ and $Z_{\text{IR}}^{\text{FDH}}$ is in the perturbative coefficients of Γ and the beta function [88–91]. However, the structure of Z_{IR} and the basic ideas remain the same. With $Z_{\text{IR}}^{\text{FDH}}$ known, we repeat the calculation of the one-loop matrix element in FDH and can obtain $\mathcal{M}_n^{(2)}$ in the FDH scheme, using (2.12).

In figure 2, we plot the finite part of the matrix element $\mathcal{M}_n^{(2)}(m=0)$, defined in (2.4), computed in the FDH scheme, using the same convention to define the finite part as in [92]. Rather than showing the dependence in the whole s-t plane, we focus on the kinematic ranges we will use in section 3, i.e. we fix $s = 174\,684\,\text{MeV}^2$ and consider the range $t \in [-153\,069, -1\,021]\,\text{MeV}^2$. This allows us also to demonstrate the split into the different contributions (cf. (2.10)). Note that, since $\mathcal{M}_n^{(2)}(m=0)$ is unphysical unless combined with real corrections, we cannot make any statements about the relative sizes of the different contributions. However, we can illustrate the numerical stability of the analytic expressions, which are provided in the supplementary material.

2.3.5 Massification

In this subsection we describe the only approximation we make for our NNLO result. It concerns the m dependence of the terms $\{q^3Q^5, q^4Q^4, q^5Q^3\}$ of $\mathcal{M}_n^{(2)}$ that are required for $\mathrm{d}\sigma_{e\mu}^{(\text{vv})}$. Starting from the corresponding matrix element with a massless electron, $\mathcal{M}_n^{(2)}(m=0)$, we can obtain the leading term of the small-mass expansion efficiently using the strategy of massification [34, 36, 37]. This way, we can recover all terms of $\mathcal{M}_n^{(2)}(m)$ that are not polynomially suppressed, i.e. the logarithmically enhanced ones as well as the constant terms, without the need of additional process-dependent computations. However, the approximation neglects terms that vanish in the limit $m \to 0$. Hence, in our result for the mixed corrections $\mathrm{d}\sigma_{e\mu}^{(2)}$ we will miss terms of the form $(\alpha/\pi)^2\, m^2/S$, potentially multiplied by a logarithm of the form $\log(m^2/S)$.

Massification is applicable in the case where some external fermions have small masses compared to all other scales in the process. Since this corresponds to highly-energetic particles in the external states, soft-collinear effective theory (SCET) [93–95] can be used for a systematic expansion of scattering amplitudes. As a consequence of the decoupling transformation [93], collinear and soft degrees of freedom factorise at leading power and we have

$$\mathcal{A}_n(m) = \Big(\prod_j \sqrt{Z}\Big) \times \mathcal{S} \times \mathcal{A}_n(0) + \mathcal{O}(m)\,. \tag{2.13}$$

Each energetic external particle defines a collinear sector in SCET and thus contributes one power of the massification constant $\sqrt{Z}$. This process-independent factor does not depend on any hard scale and apart from the trivial factorised m dependence is a constant. The soft function $\mathcal{S}$, on the other hand, is not universal and does depend on the hard scales of the process. One can show that in QED it only receives contributions from closed fermion loops [36]. As previously mentioned, these contributions can be calculated at NNLO with exact mass dependence using the semi-numerical hyperspherical method. This has the added advantage of rendering massification completely process independent.

While it is in principle possible to study these structures directly in SCET, it is easier to instead perform a matching calculation. In [37], we have explicitly calculated the leading

JHEP01(2023)112

bottom-mass effects for the process $t \to Wb$ using the method of regions [96] and were able to write the resulting amplitude as

$$\mathcal{A}_n(t \to Wb, m) = \sqrt{Z} \times \mathcal{S} \times \mathcal{A}_n(t \to Wb, 0) + \mathcal{O}(m)\,. \tag{2.14}$$

Through trivial modifications of the colour factors, this result can be converted to the QED case $\mu \to \nu\bar{\nu}e$. The exact form of the massification constant up to NNLO, i.e. $Z = 1 + Z^{(1)} + Z^{(2)}$, can be found in [37]. For photonic corrections this agrees with the expression given in [36].

We can now turn to our process and re-use Z, adding a factor of $\sqrt{Z}$ to the amplitude for each light external leg. As mentioned before, there is no soft contribution if closed fermion loops are excluded. This means that for photonic corrections to muon-electron scattering we have to write

$$\mathcal{A}_n(e\mu \to e\mu, m) = \sqrt{Z}^{\,2} \times \mathcal{A}_n(e\mu \to e\mu, 0) + \mathcal{O}(m)\,. \tag{2.15}$$

Note that Z only contains contributions due to the electron charge q and is of course independent of the muon charge Q. As for (2.11), the relation (2.15) is to be expanded in α. Since we are only using massification for the mixed contributions, it is actually sufficient to use the one-loop value of Z and we find

$$\begin{aligned} &q^4Q^2\,\mathcal{A}^{(2)}_{4,2}(m) + q^3Q^3\,\mathcal{A}^{(2)}_{3,3}(m) + q^2Q^4\,\mathcal{A}^{(2)}_{2,4}(m) \\ &= q^4Q^2\,\mathcal{A}^{(2)}_{4,2}(0) + q^3Q^3\,\mathcal{A}^{(2)}_{3,3}(0) + q^2Q^4\,\mathcal{A}^{(2)}_{2,4}(0) + Z^{(1)}\left(q^2Q^2\,\mathcal{A}^{(1)}_{2,2}(0) + qQ^3\,\mathcal{A}^{(1)}_{1,3}(0)\right). \end{aligned} \tag{2.16}$$

Massification was previously used [34, 36, 38, 56] to calculate mass effects in Bhabha and Møller scattering. It was also verified in the case of the muon decay that the massified result at NNLO gives a very good approximation to the result with exact m dependence [27].

2.4 Computing

All the contributions described in the previous paragraphs are implemented in McMule [97], a framework for (IR-safe) fully differential higher-order QED calculations. The code is publicly available at

https://gitlab.com/mule-tools/mcmule

A general presentation of McMule and of the methods employed therein is given in [26, 57, 92]. In particular, section 5 of [26] deals with the implementation of the electronic corrections at NNLO. Here the description is focused on the peculiarities of the new muon-electron scattering implementation, which completes the previous one.

The customary split of the radiative corrections into fermionic and photonic contributions is also reflected by the structure of the code. The user is allowed to choose which contributions, or pieces in the McMule notation, are to be computed. Each of the two classes is further split in terms of electronic, muonic and mixed corrections.

The non-radiative pieces are relatively straightforward to integrate over their simple phase space as there are no numerical issues. However, there is one subtlety related to the

JHEP01(2023)112

double-virtual mixed photonic piece: the matrix element is expressed in terms of several thousand GPLs. While these can be efficiently evaluated using the latest version (`v0.2.0b`) of `handyG` [98], evaluation is still limited to roughly 1 s/event. However, due to the simplicity of the actual phase-space integration that only requires $\sim 2 \times 10^5$ points, it is still possible to obtain very good results in a reasonable amount of time. A more aggressive and efficient caching system in `handyG` might improve this further.

The radiative pieces have comparatively simpler matrix elements but a more complicated phase space that tends to lead to numerical instabilities. The main issue here is the real-virtual matrix element which is evaluated using OpenLoops and NTS stabilisation (see section 2.2). For points in the bulk of the phase space, evaluation takes roughly 3 ms/event. However, the complexity of the phase space necessitates roughly 1.5×10^8 points meaning that the total integration time is on par with the non-radiative pieces.

The whole set of results can be found in the relevant directory of the McMule user library,

https://mule-tools.gitlab.io/user-library/

along with user, menu and configuration files, and the Python code that generates the plots in the paper [99]. The production runs employed version `v0.3.1` (for $\mu^- e \to \mu^- e$) and `v0.4.2` (for $\mu^+ e \to \mu^+ e$) of the McMule public release, which was encapsulated in a `docker` environment in order to ensure complete reproducibility of the results. In order to obtain a relative accuracy better than at least 10^{-4} (10^{-3}) for the NLO (NNLO) coefficient, we ran McMule for a total of 2.5 CPU-years per configuration on Intel Xeon Gold 6152 CPUs. In total, the results presented in this paper, including the checks in section 4, correspond to a runtime of roughly 21 CPU-years.[2]

3 Results

This section presents some results for muon-electron scattering at NNLO, with the characteristics of the MUonE experiment in mind. The kinematics of the process is defined by the momenta in (2.1) together with the electron and the muon mass, m and M. The Mandelstam invariants are introduced as $t_e = (p_1 - p_3)^2$ and $t_\mu = (p_2 - p_4)^2$, along with the outgoing electron and muon energy, E_e and E_μ, and the electron and muon scattering angle with respect to the beam axis, θ_e and θ_μ. If the process is elastic $t_e = t_\mu \equiv t$.

The muon beam energy is set to $E = 160\,\text{GeV}$, consistent with the M2 beam line at CERN North Area [2].[3] This corresponds to a centre-of-mass energy of $\sqrt{s} \approx 420\,\text{MeV}$. A cut is imposed on the energy of the outgoing electron, $E_e > 1\,\text{GeV}$, which is equivalent to a cut on the minimal value of $|t|$, in order to cure the singular behaviour of $\mathrm{d}\sigma/\mathrm{d}t \sim t^{-2}$. A cut on θ_μ can be used to remove most of the background. Hence, for some of our results we also require $\theta_\mu > 0.3\,\text{mrad}$.

[2] Using [100] we estimate that this corresponds to an energy consumption of 2.77 MWh and a carbon footprint of 32 kgCO_2e.

[3] This is different than the value used in previous works [21, 26] where $E = 150\,\text{GeV}$.

JHEP01(2023)112

	$E_e > 1\,\text{GeV}$	$\theta_\mu > 0.3$ mrad	$0.9 < \theta_\mu/\theta_\mu^{\text{el}} < 1.1$
S1	✓	✓	
S2	✓	✓	✓
S1'	✓		
S2'	✓		✓

Table 1. Kinematical scenarios analysed in the McMule prediction.

In order to achieve a well-defined extraction of the HVP, a possible way to proceed is to discriminate elastic scattering events from the otherwise kinematically allowed radiative events and processes in the background. This can be obtained in terms of the elasticity constraint that relates muon and electron scattering angles in the absence of photons,

$$\tan\theta_\mu^{\text{el}} = \frac{2\tan\theta_e}{(1+\gamma^2\tan^2\theta_e)(1+g_\mu^*)-2}\,, \tag{3.1}$$

where

$$\gamma = \frac{E+m}{\sqrt{s}}\,, \qquad g_\mu^* = \frac{Em+M^2}{Em+m^2}\,. \tag{3.2}$$

Applying an elasticity cut, such as

$$0.9 < \frac{\theta_\mu}{\theta_\mu^{\text{el}}} < 1.1\,, \tag{3.3}$$

would then allow to reconstruct the HVP momentum flow on an event-by-event basis. Furthermore, the cut is expected to flatten out the radiative corrections at the differential level due to an evenly distributed soft enhancement. Since MUonE plans to exploit the presence of a normalisation and a signal region, this behaviour could turn out to be advantageous. The effect of the elasticity cut (3.3) is very similar to the acoplanarity cut introduced in [22].

However, such a kinematical constraint is not ideal from the experimental perspective. It would cut off many events, yielding issues in terms of statistics, and would also complicate the estimate of systematic uncertainties, as it would lead to a complex practical implementation. At present, the alternative proposed by the experiment is to employ a template fit to extract the HVP, as discussed in [3]. Nonetheless, a study with the elasticity cut is still of theoretical interest.

In the following, results are presented for different scenarios, defined in terms of the kinematical cuts discussed above and summarised in table 1. All the results use the input parameters [101]

$$\alpha = 1/137.035999084\,, \qquad m = 0.510998950\text{ MeV}\,,$$
$$M = 105.658375\text{ MeV}\,, \qquad m_\tau = 1776.86\text{ MeV}\,.$$

The Fortran library `alphaQED` [64], in particular the most recent version `alphaQEDc19`, is employed for the evaluation of the HVP.

JHEP01(2023)112

The order-by-order contributions, $\sigma^{(i)}$, to the N^{k}LO integrated cross section, $\sigma_k = \sum_{i=0}^{k} \sigma^{(i)}$, are shown in tables 2 and 3, divided according to (2.8). The NLO hadronic piece, $\sigma^{(1)}_{\text{had}}$, corresponds to the signal of the MUonE experiment. In addition, the tables show the K factor corresponding to each contribution, defined as

$$K^{(i)} = 1 + \delta K^{(i)} = \frac{\sigma_i}{\sigma_{i-1}} \,. \tag{3.4}$$

When applicable, the tables present the different cross sections for both negative and positive muons. The mixed photonic NLO correction with positive muons can be derived from the one with negative muons by flipping the sign of the latter. The mixed photonic NNLO correction could be further disentangled into three classes, labelled by the leptonic charges relative to the LO cross section, i.e. $\{q^3\,Q,\, q^2\,Q^2,\, q\,Q^3\}$, so that the contribution with positive muons can be derived from the one with negative muons by flipping the sign of the classes with odd powers of Q. Once all mixed contributions are added up as displayed in the tables, this symmetry is not manifest anymore.

According to table 2, NLO and NNLO corrections amount to around 1% and 0.01% (or less) for `S1`, and to around 3% and 0.01% for `S2`. The elasticity constraint cuts off hard radiation and the consequent soft enhancement introduces large logarithms that result in larger K ratios in the latter scenario, particularly in the case of electronic corrections. For `S1` there is no apparent hierarchy among photonic corrections, while leptonic contributions, especially those due to electronic VP insertions, dominate NLO and NNLO corrections. For `S2` a hierarchy between electronic and mixed photonic contributions, both at NLO and at NNLO, is more evident.

Comparing table 3 and table 2 reveals that the cut on θ_μ has a large impact on NLO corrections, similar to the elasticity cut. However, the θ_μ cut has a much more pronounced effect on the total cross section, as it also affects the Born term.

In addition to integrated cross sections, differential distributions can provide a more reliable estimate with respect to MUonE's 10 ppm target, as higher-order corrections can be much larger at that level. As a Monte Carlo integrator, McMule allows for the calculation of any number of IR-safe differential observables in the same run. Here,[4] figures 3–5 display differential results that are of interest to the MUonE experiment, in particular distributions with respect to θ_e and θ_μ. The differential cross sections at LO and NNLO are shown in the upper panels. Furthermore, the lower panels show the differential K factor

$$\delta K^{(i)} = \frac{\mathrm{d}\sigma^{(i)}/\mathrm{d}x}{\mathrm{d}\sigma_{i-1}/\mathrm{d}x} \,, \tag{3.5}$$

with $x \in \{\theta_e, \theta_\mu\}$. From top to bottom, the second panel displays the NLO K factor for negative muons, the third and fourth panel the NNLO K factor for negative and positive muons, the fifth panel again the NNLO K factor for negative muons restricted to mixed photonic contributions, further disentangled in terms of the three gauge-invariant subsets, labelled by their leptonic charge.

[4] Results for other observables can be found in the McMule User Library.

JHEP01(2023)112

	$\sigma/\mu b$		$\delta K^{(i)}/\%$	
	S1	S2	S1	S2
σ_0	106.44356	106.44356		
$\sigma_e^{(1)}$	−0.61211(3)	−4.66042(3)	−0.57506(3)	−4.37830(3)
$\sigma_{e\mu}^{(1)}$ −	−0.21404	−0.16017	−0.20108	−0.15047
$\sigma_{e\mu}^{(1)}$ +	0.21404	0.16017	0.20108	0.15047
$\sigma_\mu^{(1)}$	−0.02843	−0.16134	−0.02671	−0.15157
$\sigma_{\text{lep}}^{(1)}$	1.38575	1.38575	1.30186	1.30186
$\sigma_{\text{had}}^{(1)}$	0.01565	0.01565	0.01471	0.01471
σ_1 −	106.99038(3)	102.86304(3)	0.51372(3)	−3.36377(3)
σ_1 +	107.41847(3)	103.18338(3)	0.91589(3)	−3.06283(3)
$\sigma_e^{(2)}$	0.00090	0.06595	0.00084	0.06411
$\sigma_{e\mu}^{(2)}$ −	0.00095	0.01926	0.00089	0.01872
$\sigma_{e\mu}^{(2)}$ +	0.00329	0.00479	0.00307	0.00464
$\sigma_\mu^{(2)}$	−0.00005	0.00002	−0.00005	0.00002
$\sigma_{\text{lep}}^{(2)}$ −	−0.01195	−0.06568	−0.01117	−0.06385
$\sigma_{\text{lep}}^{(2)}$ +	−0.00424	−0.05959	−0.00395	−0.05775
$\sigma_{\text{had}}^{(2)}$ −	−0.00045	−0.00104	−0.00042	−0.00101
$\sigma_{\text{had}}^{(2)}$ +	−0.00004	−0.00068	−0.00004	−0.00066
σ_2 −	106.97977(3)	102.88154(3)	−0.00992(4)	0.01799(4)
σ_2 +	107.41832(3)	103.19386(3)	−0.00013(4)	0.01016(4)

Table 2. Integrated cross sections for S1 and S2 at LO, NLO, and NNLO. The results are split into photonic, i.e. electronic, mixed and muonic, and fermionic, i.e. leptonic and hadronic, corrections. All three leptons are included in the leptonic contributions. When applicable, the different contributions with negative and positive muons are shown. Where no error is given, all digits are significant compared to the precision of the numerical integration.

In the case of the θ_e distribution, (N)NLO corrections can be larger at differential level, for example up to 20% (0.2%), as shown in figure 3. These large corrections occur for small electron scattering angles, or equivalently for large electron energies, where photon emission is forced to be soft. Furthermore, the effect of the elasticity cut is clearly visible when comparing figure 3 and figure 4. As expected from an evenly-distributed soft enhancement, the K factor is significantly flattened.

Among photonic corrections, a hierarchy is expected from the appearance of collinear pseudo-singularities. At the cross section level, this introduces logarithms of the form $\log(m_i^2/S)$, where $m_i \in \{m, M\}$ and S is the energy scale of the process. As a consequence, electronic corrections are expected to be dominant compared to mixed corrections, and even more compared to muonic corrections.

JHEP01(2023)112

	$\sigma/\mu\text{b}$		$\delta K^{(i)}/\%$	
	S1'	S2'	S1'	S2'
σ_0	245.59625(1)	245.59625(1)		
$\sigma_e^{(1)}$	10.8488(2)	−11.18183(7)	4.41735(7)	−4.55293(3)
$\sigma_{e\mu}^{(1)}$ −	−0.35021	−0.28598	−0.14260	−0.11644
$\sigma_{e\mu}^{(1)}$ +	0.35021	0.28598	0.14260	0.11644
$\sigma_\mu^{(1)}$	−0.06668	−0.22413	−0.02715	−0.09126
$\sigma_{\text{lep}}^{(1)}$	2.88969	2.88969	1.17660	1.17660
$\sigma_{\text{had}}^{(1)}$	0.01943	0.01943	0.00791	0.00791
σ_1 −	258.9373(2)	236.81343(7)	5.43211(7)	−3.57612(3)
σ_1 +	259.6377(2)	237.38539(7)	5.71731(7)	−3.34324(3)
$\sigma_e^{(2)}$	0.02713(4)	0.17491(1)	0.01048(2)	0.07386
$\sigma_{e\mu}^{(2)}$ −	−0.02526	0.02852	−0.00975	0.01204
$\sigma_{e\mu}^{(2)}$ +	0.03165	0.00439	0.01219	0.01852
$\sigma_\mu^{(2)}$	−0.00010	−0.00004	−0.00004	−0.00002
$\sigma_{\text{lep}}^{(2)}$ −	0.05911	−0.13445	0.02283	−0.05678
$\sigma_{\text{lep}}^{(2)}$ +	0.07161	−0.12380	0.02758	−0.05215
$\sigma_{\text{had}}^{(2)}$ −	−0.00049	−0.00128	−0.00019	−0.00054
$\sigma_{\text{had}}^{(2)}$ +	0.00000	−0.00083	0.00000	−0.00035
σ_2 −	258.9977(2)	236.88109(7)	0.02332(9)	0.02857(4)
σ_2 +	259.7680(2)	237.44002(7)	0.05018(9)	0.02301(4)

Table 3. Integrated cross sections for S1' and S2' at LO, NLO, and NNLO. The results are split into photonic, i.e. electronic, mixed and muonic, and fermionic, i.e. leptonic and hadronic, corrections. All three leptons are included in the leptonic contributions. When applicable, the different contributions with negative and positive muons are shown. Where no error is given, all digits are significant compared to the precision of the numerical integration.

This phenomenon can be observed at NLO, where the electronic contribution is the largest, and particularly for S1, where the additional soft enhancement at the endpoints of the distributions seems to affect the electronic correction even more.

The collinear hierarchy is less pronounced at NNLO, apparently because of further enhancements of soft origin. In fact, electronic and mixed corrections are similar in magnitude for small θ_e, where the soft enhancement is prevalent. Nonetheless, the collinear hierarchy is partially restored in the bulk of the distribution. The interplay between collinear and soft enhancements is even clearer from the lowest panel in figure 3, where the soft enhancement of the mostly-electronic mixed correction (q^3Q) turns out to account for the similar magnitude of electronic and mixed corrections for small θ_e. Similarly, NNLO results for S2 in figure 4 are further enhanced by soft logarithms because of the additional elasticity constraint. As a consequence, the collinear hierarchy is less visible in the bulk of the distribution.

JHEP01(2023)112

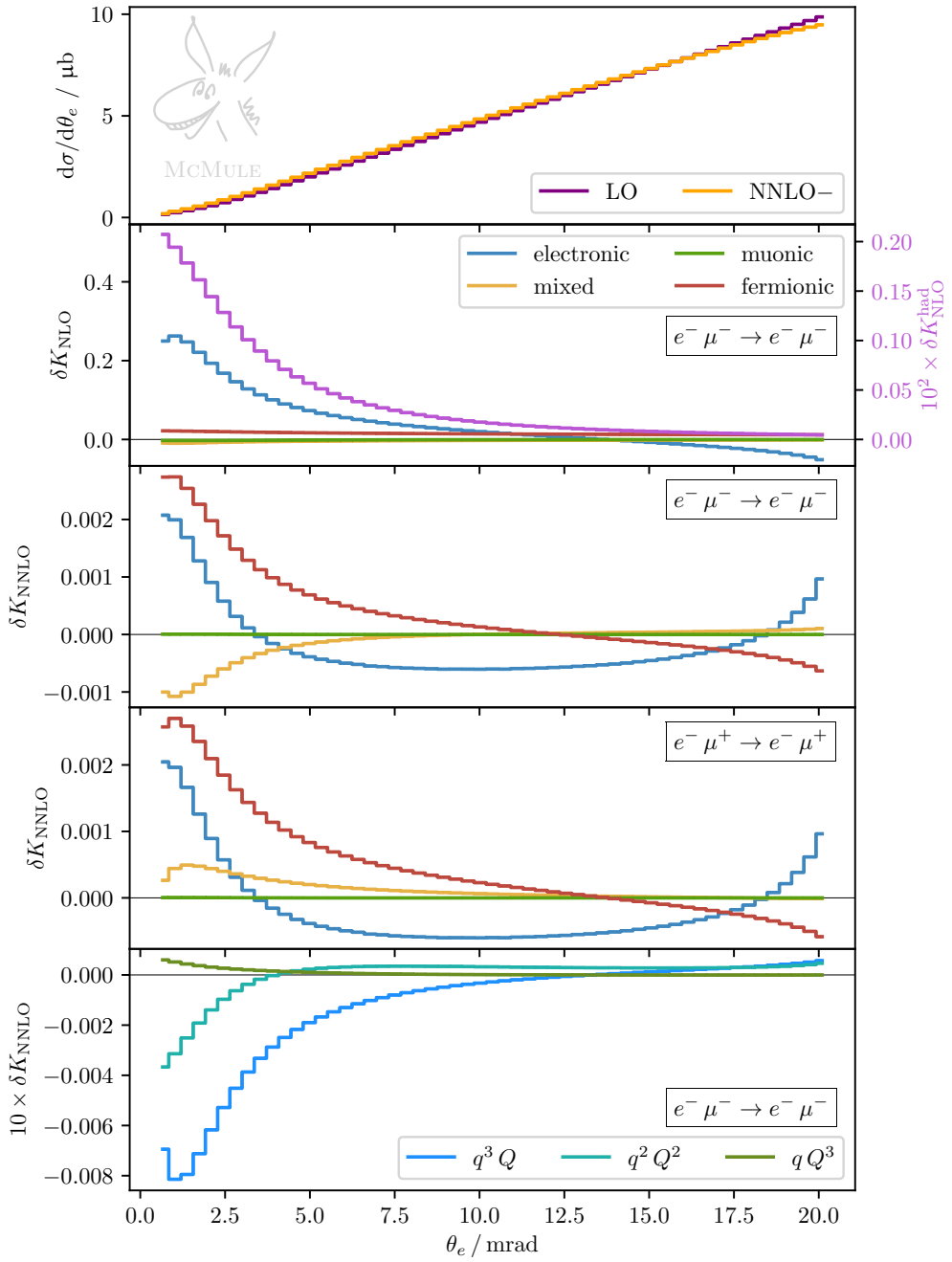

Figure 3. From top to bottom: (i) differential cross section w.r.t. θ_e for `S1` at LO (violet), and NNLO (orange) for negative muons; (ii) NLO K factor for negative muons (positive muons have a sign flip for the mixed photonic correction); (iii) NNLO K factor for negative muons; (iv) NNLO K factor for positive muons; (v) NNLO K factor for disentangled mixed photonic corrections, for negative muons. In panels (ii)–(iv) the correction is split into photonic, i.e. electronic, mixed and muonic, and fermionic, including leptonic and hadronic. The hadronic correction at NLO corresponds to the signal of the experiment and is shown separately in purple in panel (ii).

JHEP01(2023)112

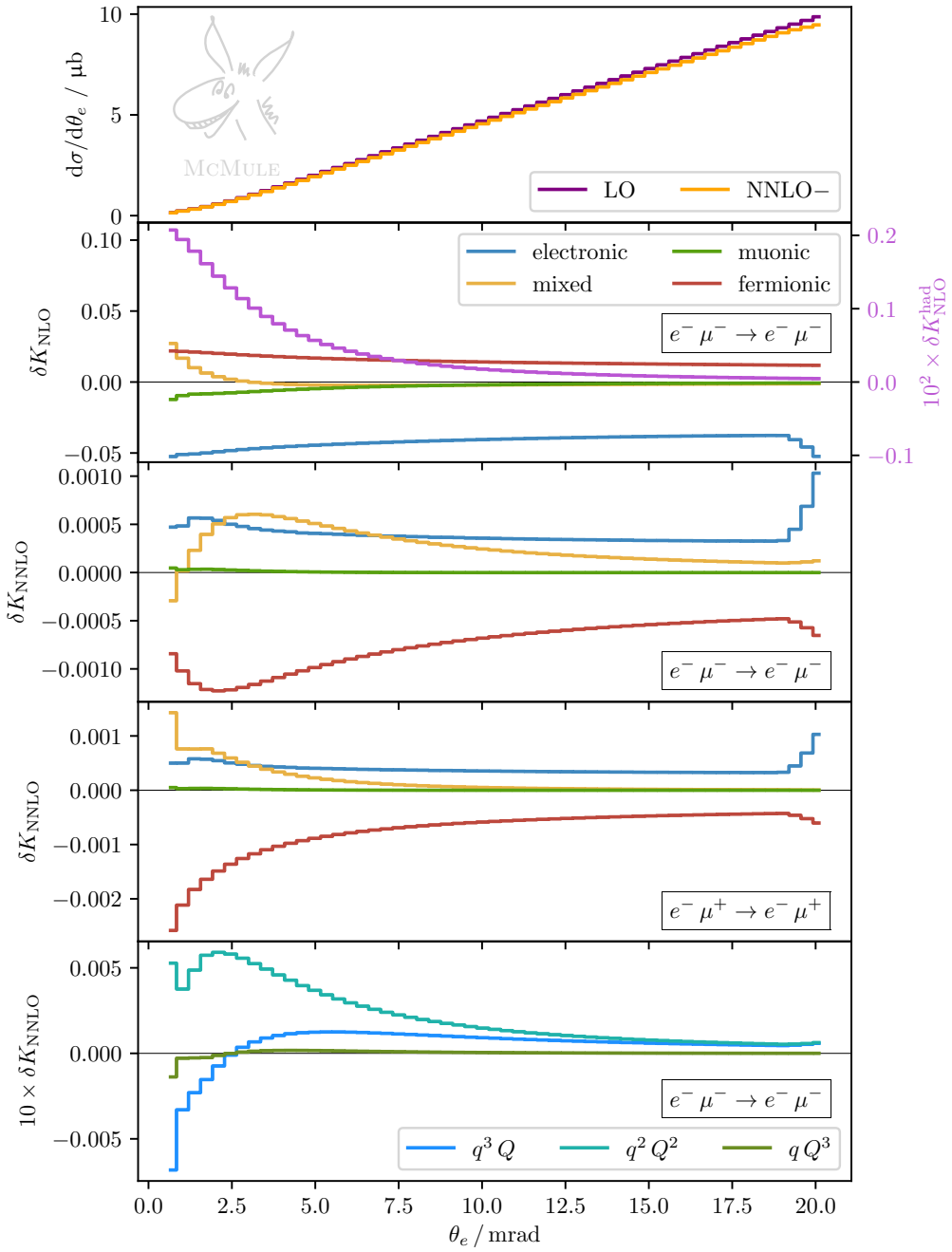

Figure 4. From top to bottom: (i) differential cross section w.r.t. θ_e for `S2` at LO (violet), and NNLO (orange) for negative muons; (ii) NLO K factor for negative muons (positive muons have a sign flip for the mixed photonic correction); (iii) NNLO K factor for negative muons; (iv) NNLO K factor for positive muons; (v) NNLO K factor for disentangled mixed photonic corrections, for negative muons. In panels (ii)–(iv) the correction is split into photonic, i.e. electronic, mixed and muonic, and fermionic, including leptonic and hadronic. The hadronic correction at NLO corresponds to the signal of the experiment and is shown separately in purple in panel (ii).

JHEP01(2023)112

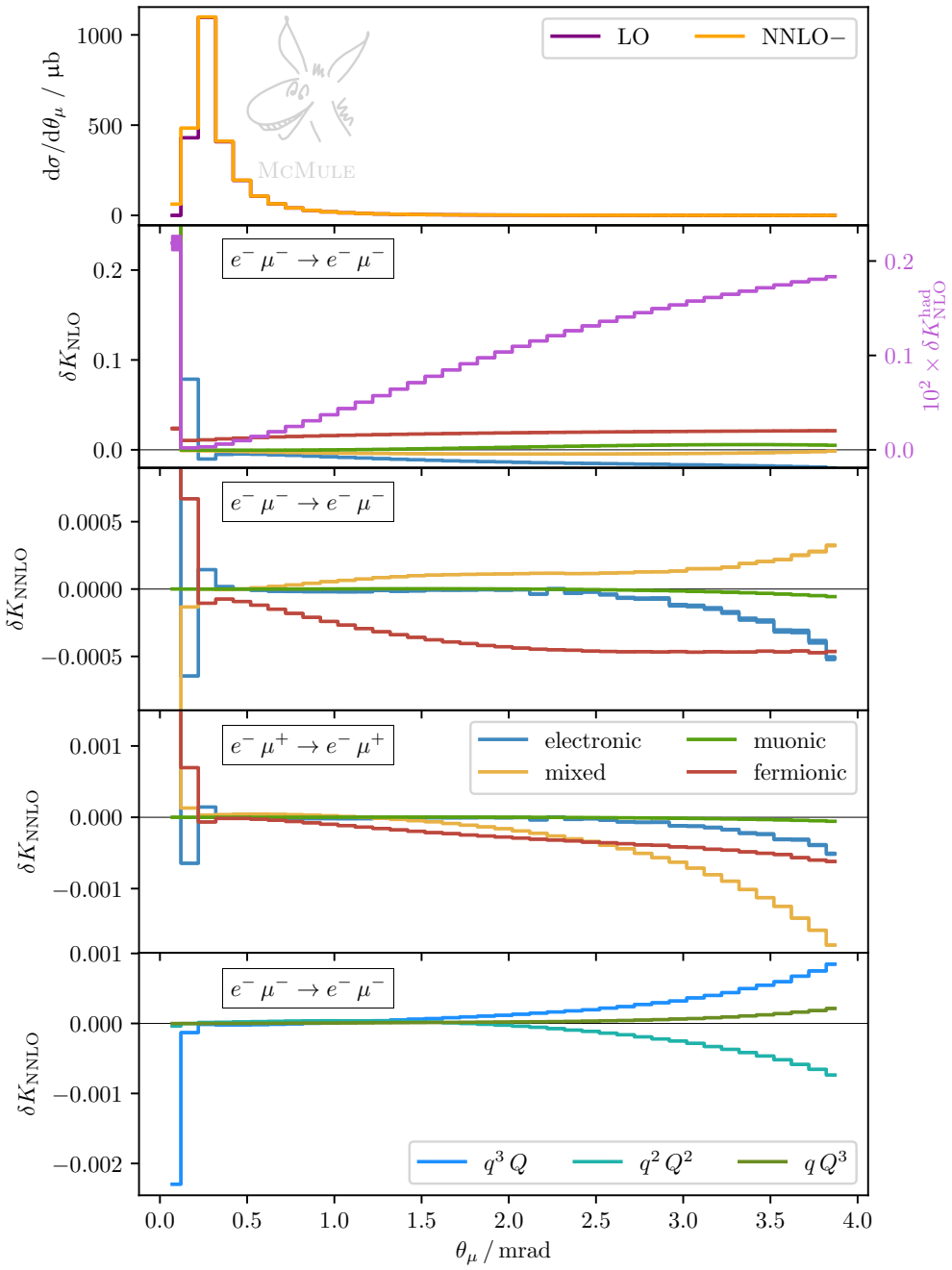

Figure 5. From top to bottom: (i) differential cross section w.r.t. θ_μ for `S1`' at LO (violet), and NNLO (orange) for negative muons; (ii) NLO K factor for negative muons (positive muons have a sign flip for the mixed photonic correction); (iii) NNLO K factor for negative muons; (iv) NNLO K factor for positive muons; (v) NNLO K factor for disentangled mixed photonic corrections, for negative muons. In panels (ii)–(iv) the correction is split into photonic, i.e. electronic, mixed and muonic, and fermionic, including leptonic and hadronic. The hadronic correction at NLO corresponds to the signal of the experiment and is shown separately in purple in panel (ii).

JHEP01(2023)112

In the case of the θ_μ distribution in `S1'`, displayed in figure 5, a strong enhancement for small values of θ_μ is visible for all NLO and NNLO K factors, except for the NLO fermionic. This explains why MUonE enforces a kinematical cut for small muon scattering angles, in order not to lose the majority of these events. On the other hand, fermionic corrections at NLO are not enhanced (note the different scale for the NLO hadronic), since NLO fermionic corrections correspond to elastic events, which are not affected by the cut at $\theta_\mu = 0.3$ mrad.

Finally, figure 3 and figure 5 also show that the MUonE signal, i.e. the hadronic NLO corrections, are $\mathcal{O}(10^{-3})$ in the regions of small θ_e and large θ_μ.

However, the magnitude of NNLO corrections at differential level, around 10^{-3}, is still too large compared to MUonE's precision goal of 10 ppm. Higher-order predictions beyond NNLO can certainly help in that direction. Furthermore, it is clearly mandatory to make an effort towards a more reliable description of the region where radiation leads to an enhancement through large logarithms.

4 Checks and validation

Since this paper presents the first full prediction for muon-electron scattering at NNLO in QED, various studies were conducted in order to validate the results. Checks were performed both externally (section 4.1), against independent though partial results, and internally (section 4.2), in order to test the consistency and the validity of the methods. In particular, both photonic and fermionic NNLO corrections could be completely tested against independent calculations, except for the contribution of the two-loop four-point topologies to the mixed photonic correction.

4.1 External checks

The electronic and muonic contributions to the photonic NNLO correction were also calculated in [21] with Mesmer. Since a slicing scheme is employed therein to handle IR divergences, along with a photon-mass regulator, a comparison with McMule represents a completely independent check. A positive outcome was reported in [26]. As mentioned in section 2.2, we have improved upon this calculation by using OpenLoops combined with NTS stabilisation to evaluate the real-virtual contribution. This yields a better convergence behaviour of the Monte Carlo integration. Perfect agreement with the Mesmer results is also found in this case.

For the mixed photonic NNLO result, a new comparison was conducted with the Mesmer collaboration. Since the calculation in [21] is complete up to the mixed two-loop contribution, it is possible to compare the mixed NLO correction to $\mu e \to \mu e \gamma$, which is physical and corresponds to the double-real and real-virtual contributions to muon-electron scattering. In order to check the numerical stability of the real-virtual implementation, small photon energy cuts of $\{10^{-6}, 10^{-5}, 10^{-4}\} \times \sqrt{s}/2$ were used. Perfect agreement was found between the two codes for the total cross section as well as for differential distributions.

A verification of the complete NNLO calculation and in particular of the genuine two-loop four-point topologies with Mesmer is currently not possible. In [21] these contributions were approximated with a YFS-inspired approach. Since this only yields

JHEP01(2023)112

a rough estimate of the exact result, a meaningful comparison is not viable. Instead, we have made an independent test of the massified two-loop matrix element. To this end, we start from a completely independent massless calculation of the matrix element for Bhabha scattering [102]. We restrict the result to the t-channel [38] contribution and massify both fermion lines. As can be expected, this result approaches the muon-electron two-loop matrix element in the high-energy limit $S \gg M, m$. This represents a strong check on the correctness of the massless two-loop matrix element as well as the consistency of the massification procedure.

Finally, the fermionic contribution to the NNLO correction was also computed in [12] through a dispersive approach, using e^+e^- annihilation data for the hadronic part. On the other hand, the McMule implementation employs the hyperspherical results from [13]. The positive outcome of the comparison between the two sets of results, for both leptonic and hadronic distributions, constitutes an additional strong validation.

4.2 Internal checks

Further checks were performed internally to test the new ingredients of the present calculation and are discussed with more details in the following subsections. In particular, section 4.2.1 presents a validation for the Fortran implementation in McMule, section 4.2.2 analyses the effect of massification, and section 4.2.3 studies the impact of NTS stabilisation applied to the calculation of real-virtual contributions. The results of all of these checks are summarised in figure 6.

4.2.1 Implementation

In addition to the external checks, a validation for the Fortran implementation is provided through the subtraction method employed by McMule. As given in (2.7), FKS$^\ell$ introduces the unphysical parameter ξ_c, on which the three pieces contributing to the photonic NNLO correction (double-virtual, real-virtual and double-real) depend. The cancellation of the ξ_c dependence, when the three pieces are summed together, is a strong check in terms of implementation consistency and numerical stability, even more when performed at the level of differential distributions.

The second and third panel of figure 6 show, for a number of merged bins, the relative difference between the differential cross section computed for each of the ξ_c employed for the calculation (ξ_i) and the combined differential cross section (labelled with ξ_c), for the electronic and the mixed NNLO correction in `S1`, respectively.

The error bars in the plot indicate very good consistency and stability of the implementation, on top of (unavoidable) larger oscillations corresponding to the zero crossings of the distributions.

4.2.2 Massification error

It is essential to validate the reliability of the approximation provided by massification for the considered observables. To do so, one can use the electronic NNLO correction, computed with full mass dependence, to obtain an error estimate when massification is applied to the massless two-loop electron form factor.

JHEP01(2023)112

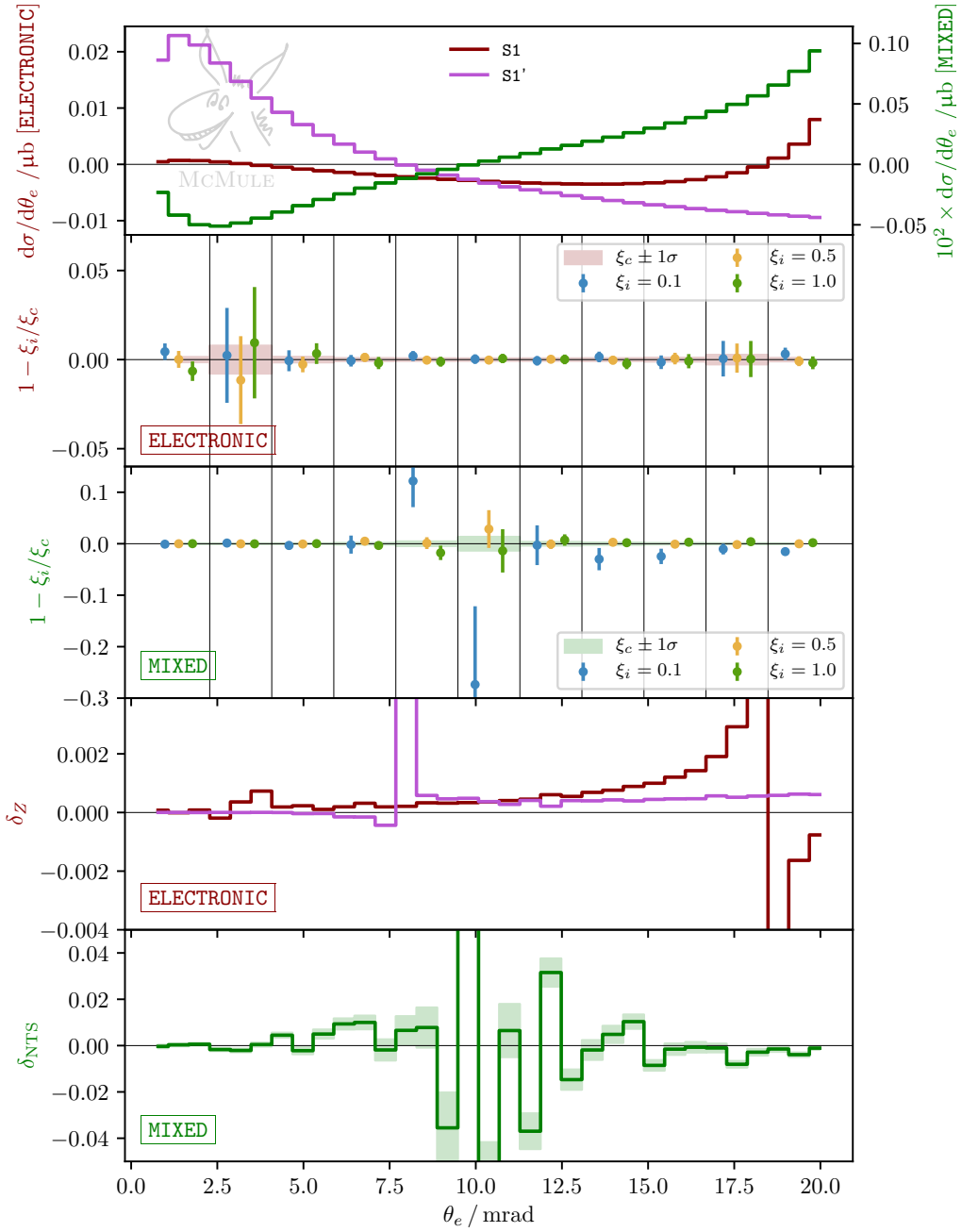

Figure 6. Validation plots for electronic and mixed photonic corrections, as differential distributions w.r.t. the electron scattering angle. From top to bottom (see the corresponding subsections in section 4 for further details): (i) differential NNLO correction w.r.t. θ_e — electronic in `S1` in red, electronic in `S1'` in purple, mixed in `S1` in green; (ii) ξ_c-(in)dependence study for NNLO electronic corrections in `S1`; (iii) ξ_c-(in)dependence study for NNLO mixed corrections in `S1`; (iv) massification study for NNLO electronic corrections — `S1` in red, `S1'` in purple; (v) NTS stabilisation study for NNLO mixed corrections. See (4.2) and (4.3) for details on δ_Z and δ_{NTS}.

JHEP01(2023)112

We write the massified electronic NNLO corrections as

$$\mathrm{d}\tilde{\sigma}_e^{(2)}(m) = (1+\delta_Z)\,\mathrm{d}\sigma_e^{(2)}(m) \tag{4.1}$$

and thereby introduce the relative difference, δ_Z, between the NNLO coefficients of the full and massified electronic correction. The second-to-last panel of figure 6 shows δ_Z in two different scenarios, `S1` and `S1`', which differ for the enforcement of an additional cut on the muon scattering angle, $\theta_\mu > 0.3$ mrad $\equiv \theta_\mu^c$. We stress that the difference between the massified and full result for the NNLO coefficients only affects the double-virtual contributions, which are computed with and without massification, respectively.

The relative difference at the level of the NNLO differential cross section is

$$\frac{\mathrm{d}\tilde{\sigma}_2 - \mathrm{d}\sigma_2}{\mathrm{d}\sigma_2} = \frac{\mathrm{d}\sigma_e^{(2)}}{\mathrm{d}\sigma_2}\,\delta_Z \sim \alpha^2\,\delta_Z\,, \tag{4.2}$$

i.e. at most around $10^{-3}\alpha^2$ in the present case, so that we can safely argue that massification is not providing a source of uncertainty in the context of MUonE's precision goal of 10 ppm. The error bars are not visible since they are much smaller than the scale of δ_Z. In particular, they quantify the error of the ratio between the double-virtual contributions to the massified and the full NNLO correction. This error is at least a thousand times smaller than the Monte Carlo error of the physical NNLO corrections, not shown in the plot.

However, in the case of `S1`, δ_Z seems to increase for $\theta_e \sim 15$ mrad, on top of (unavoidable) larger oscillations due to the zero crossings of the distributions. Since massification is applied to the double-virtual contribution, this behaviour can be explained with a focus on elastic events. In this respect, electron scattering angles around 15 mrad correspond to muon scattering angles around 0.5 mrad. As θ_e increases, the difference between the corresponding θ_μ and θ_μ^c gets smaller and smaller. The appearance of such a small quantity breaks the power counting massification is based on and thus results in a less reliable approximation. This observation is confirmed by the absence of a similar trend in the case of `S1`', where the same cut is not enforced, in purple in figure 6.

4.2.3 Impact of next-to-soft stabilisation

A final check validates the procedure of NTS stabilisation, which is used for computing real-virtual contributions in phase-space regions where the evaluation with OpenLoops becomes numerically unstable.

Below a certain value of the photon energy, fixed at $10^{-3}\sqrt{s}/2$ for the present implementation, the evaluation of the real-virtual matrix element is switched to the NTS expansion. This is a much simpler and thus numerically much more stable expression. Alternatively, one can use OpenLoops in quadruple precision to always use the full matrix element for the entire phase space. This has an enormous price in terms of computing time, but can be used to validate the NTS expansion.

In analogy to (4.1) we write the NTS-expanded mixed NNLO correction as $(1+\delta_{\mathrm{NTS}})\,\mathrm{d}\sigma_{e\mu}^{(2)}$, where $\mathrm{d}\sigma_{e\mu}^{(2)}$ is computed using OpenLoops in quadruple precision for the full phase space. The last panel of figure 6 shows the relative difference δ_{NTS} at differential level. Except for oscillations due to the zero crossing of the distribution, the relative

JHEP01(2023)112

difference at the level of the NNLO differential cross section, i.e.

$$\frac{\mathrm{d}\sigma^{(2)}_{e\mu}}{\mathrm{d}\sigma_2}\,\delta_{\mathrm{NTS}} \sim \alpha^2\,\delta_{\mathrm{NTS}}\,, \tag{4.3}$$

is at most around $10^{-2}\alpha^2$. The error bars in this figure only include the error of the real-virtual contributions. We stress that this error is at least ten times smaller than the Monte Carlo integration error of the physical NNLO correction, not shown in the plot. Hence, we can safely argue that the NTS expansion is an extremely good approximation.

As a consequence, the NTS expansion accurately represents the full real-virtual contribution, as much as the full computation with OpenLoops in quadruple precision. However, it allows for a much faster integration. The data in the plot, using the same amount of statistics and the same setup for both cases, required seven days with NTS stabilisation, three months without it.

5 Conclusions and outlook

We have presented the first calculation of the complete set of NNLO QED corrections to muon-electron scattering. The results presented here constitute the first complete and fully differential NNLO calculation of a $2 \to 2$ process with two different non-vanishing masses on the external lines. They were obtained by combining state-of-the-art analytic calculations of two-loop amplitudes and their numerical evaluations with advanced QFT-inspired methods to ensure an efficient and numerically stable phase-space integration, even in the presence of a large hierarchy of scales. Through crossing, they also open the door to study muon-pair and tau-pair production at electron-positron colliders to unprecedented precision. Furthermore, they can be adapted to contribute to an improved description of lepton-proton scattering.

Our results include leptonic, non-perturbative hadronic, and photonic corrections. The fermionic matrix elements were calculated with the semi-numerical hyperspherical method, while a purely analytic approach was followed for the photonic parts. The phase-space integration is performed numerically in the McMule framework [26], where the soft singularities are subtracted using the FKS$^\ell$ scheme [27]. This allows for a fully-differential calculation of any IR-safe observable.

Electronic and muonic corrections have been computed exactly based on the analytic result for the heavy-lepton and heavy-quark form factors [54, 55]. The full mass dependence of the genuine four-point two-loop topologies, on the other hand, is currently not known. Adapting the recent computation of the two-loop matrix element for $e^+\,e^- \to \mu^+\mu^-$ [30] for massless electrons, we have computed the corresponding matrix element for muon-electron scattering. Based on this result, it was possible to reconstruct the leading electron-mass effects using massification [37]. This correctly captures both logarithmically enhanced as well as constant terms and results within an error of the order of $(\alpha/\pi)^2 m^2/S \log(m^2/S)$. It can therefore be expected that the impact of the missing terms lies well below MUonE's target precision of 10 ppm. We have substantiated this claim by comparing the massive

JHEP01(2023)112

computation for the electron line corrections with the massified result. The difference is smaller than the Monte Carlo error, which is negligible for practical purposes.

The second bottleneck in the calculation is given by the numerical (in)stability of the radiative matrix element for soft and collinear photon emission. A stable and fast implementation of the delicate real-virtual matrix element was possible by combining OpenLoops [39, 40] with NTS stabilisation [38, 41]. We have cross-checked this approach by running OpenLoops in quadruple-precision mode and found perfect agreement of the two results within the Monte Carlo error. Furthermore, the real-virtual and double-real contributions have been validated in a dedicated comparison of the radiative process with the Mesmer collaboration.

The calculation presented here represents a major milestone towards the ambitious 10 ppm precision goal of the MUonE experiment. The corresponding results unveil rather large NNLO corrections of up to $\sim 10^{-3}$, depending on the angle of the scattered electron. They are thus absolutely essential for the MUonE program. The enhancement can be traced back to the presence of soft logarithms. An inclusion of these effects beyond NNLO is therefore unavoidable to reach the required precision. The leading logarithms can be resummed with a parton shower and a corresponding effort is ongoing to extend the McMule framework accordingly.

Even with a NNLO-matched parton shower it will be essential to reliably assess the impact of missing higher-order contributions. An analytic approach to resum next-to-leading logarithmic effects could therefore be helpful in this regard. It is, however, unlikely that this can be done for realistic MUonE observables. An alternative approach is given by the fixed-order calculation of the electron-line corrections at N^{3}LO. With the all-order subtraction scheme FKS$^\ell$ and the recent calculation of the heavy-quark form factor at three loop [103, 104] such an endeavour indeed seems feasible. The main missing piece is the real-virtual-virtual matrix element which is only known for massless electrons [105, 106]. As an alternative route to an analytic calculation of this matrix element, one could follow a numerical approach to calculate the loop integrals using e.g. DiffExp [107], AMFlow [108], or SecDec [109]. Another option is to extend massification to radiative processes. A corresponding collaborative effort has been launched recently [110].

Last but not least, a rigorous assessment of the reliability of the massified approximation is clearly desirable. A computation with full mass dependence is therefore envisaged. Analytic results for a subset of the planar master integrals have recently become available [111]. A numerical approach seems, however, more promising in this case. In fact, similar techniques as for the electronic real-virtual-virtual amplitude might also be applicable here. The N^{3}LO endeavour will therefore not only control missing higher-order effects but might also facilitate the fully-massive NNLO calculation. A prediction of the SM background for MUonE with the ambitious target precision of 10 ppm thus seems within reach in the near-term future.

Acknowledgments

We are pleased to acknowledge the Theory Group of the MUonE initiative/experiment. In particular, Massimo Passera, for his constant support and stimulating discussions, as well

JHEP01(2023)112

as for collaboration at early stages; Carlo Carloni, Matteo Fael, Guido Montagna, Fulvio Piccinini, for interesting discussions and comparisons, at various stages.

We are grateful to the Mainz Institute of Theoretical Physics (MITP) of the DFG Cluster of Excellence PRISMA$^+$ (Project ID 39083149) for its hospitality during the workshop "The Evaluation of the Leading Hadronic Contribution to the Muon $g-2$: Toward the MUonE Experiment".

The work of A.B. was supported in part by the ERC Starting Grant REINVENT-714788. T.E. and M.R. acknowledge support from the Swiss National Science Foundation (SNSF) under grant 200020_207386. The work of A.F. was supported in part by the PSC-CUNY Award 64101-00 52. The work of M.K.M. is supported by Fellini - Fellowship for Innovation at INFN funded by the European Union's Horizon 2020 research and innovation programme under the Marie Skłodowska-Curie grant agreement No 754496. The work of J.R. is supported by the Italian Ministry of Research (MUR) under grant PRIN 20172LNEEZ. The work of W.J.T. received funding from the European Research Council (ERC) under the European Union's Horizon 2020 research and innovation programme (grant agreement No 725110), *Novel structures in scattering amplitudes*. Y.U. acknowledges support by the U.K. Science and Technology Facilities Council (STFC) under grant ST/T001011/1. The work of M.Z. was supported by the Swiss National Science Foundation (SNSF) under the Ambizione grant PZ00P2-179877.

References

[1] G. Abbiendi et al., *Measuring the leading hadronic contribution to the muon $g-2$ via μe scattering*, *Eur. Phys. J. C* **77** (2017) 139 [arXiv:1609.08987] [INSPIRE].

[2] MUONE collaboration, *Status of the MUonE experiment*, *PoS* **EPS-HEP2021** (2022) 642 [INSPIRE].

[3] G. Abbiendi, *Status of the MUonE experiment*, *Phys. Scripta* **97** (2022) 054007 [arXiv:2201.13177] [INSPIRE].

[4] C.M. Carloni Calame, M. Passera, L. Trentadue and G. Venanzoni, *A new approach to evaluate the leading hadronic corrections to the muon $g-2$*, *Phys. Lett. B* **746** (2015) 325 [arXiv:1504.02228] [INSPIRE].

[5] MUON G-2 collaboration, *Final report of the muon E821 anomalous magnetic moment measurement at BNL*, *Phys. Rev. D* **73** (2006) 072003 [hep-ex/0602035] [INSPIRE].

[6] MUON G-2 collaboration, *Measurement of the positive muon anomalous magnetic moment to 0.46 ppm*, *Phys. Rev. Lett.* **126** (2021) 141801 [arXiv:2104.03281] [INSPIRE].

[7] T. Aoyama et al., *The anomalous magnetic moment of the muon in the Standard Model*, *Phys. Rept.* **887** (2020) 1 [arXiv:2006.04822] [INSPIRE].

JHEP01(2023)112

[8] M. Davier, A. Hoecker, B. Malaescu and Z. Zhang, *A new evaluation of the hadronic vacuum polarisation contributions to the muon anomalous magnetic moment and to $\alpha(m_Z^2)$*, *Eur. Phys. J. C* **80** (2020) 241 [arXiv:1908.00921] [INSPIRE].

[9] A. Keshavarzi, D. Nomura and T. Teubner, *$g-2$ of charged leptons, $\alpha(M_Z^2)$, and the hyperfine splitting of muonium*, *Phys. Rev. D* **101** (2020) 014029 [arXiv:1911.00367] [INSPIRE].

[10] S. Borsanyi et al., *Leading hadronic contribution to the muon magnetic moment from lattice QCD*, *Nature* **593** (2021) 51 [arXiv:2002.12347] [INSPIRE].

[11] E. Balzani, S. Laporta and M. Passera, *Hadronic vacuum polarization contributions to the muon $g-2$ in the space-like region*, *Phys. Lett. B* **834** (2022) 137462 [arXiv:2112.05704] [INSPIRE].

[12] M. Fael and M. Passera, *Muon-electron scattering at next-to-next-to-leading order: the hadronic corrections*, *Phys. Rev. Lett.* **122** (2019) 192001 [arXiv:1901.03106] [INSPIRE].

[13] M. Fael, *Hadronic corrections to μ-e scattering at NNLO with space-like data*, *JHEP* **02** (2019) 027 [arXiv:1808.08233] [INSPIRE].

[14] A. Masiero, P. Paradisi and M. Passera, *New physics at the MUonE experiment at CERN*, *Phys. Rev. D* **102** (2020) 075013 [arXiv:2002.05418] [INSPIRE].

[15] P.S.B. Dev, W. Rodejohann, X.-J. Xu and Y. Zhang, *MUonE sensitivity to new physics explanations of the muon anomalous magnetic moment*, *JHEP* **05** (2020) 053 [arXiv:2002.04822] [INSPIRE].

[16] U. Schubert and C. Williams, *Interplay between SM precision, BSM physics, and the measurements of $\alpha_{\rm had}$ in μ-e scattering*, *Phys. Rev. D* **100** (2019) 035030 [arXiv:1907.01574] [INSPIRE].

[17] G. Grilli di Cortona and E. Nardi, *Probing light mediators at the MUonE experiment*, *Phys. Rev. D* **105** (2022) L111701 [arXiv:2204.04227] [INSPIRE].

[18] I. Galon, D. Shih and I.R. Wang, *Dark photons and displaced vertices at the MUonE experiment*, arXiv:2202.08843 [INSPIRE].

[19] K. Asai, K. Hamaguchi, N. Nagata, S.-Y. Tseng and J. Wada, *Probing the L_μ-L_τ gauge boson at the MUonE experiment*, *Phys. Rev. D* **106** (2022) L051702 [arXiv:2109.10093] [INSPIRE].

[20] P. Banerjee et al., *Theory for muon-electron scattering @10 ppm: a report of the MUonE theory initiative*, *Eur. Phys. J. C* **80** (2020) 591 [arXiv:2004.13663] [INSPIRE].

[21] C.M. Carloni Calame, M. Chiesa, S.M. Hasan, G. Montagna, O. Nicrosini and F. Piccinini, *Towards muon-electron scattering at NNLO*, *JHEP* **11** (2020) 028 [arXiv:2007.01586] [INSPIRE].

[22] M. Alacevich, C.M. Carloni Calame, M. Chiesa, G. Montagna, O. Nicrosini and F. Piccinini, *Muon-electron scattering at NLO*, *JHEP* **02** (2019) 155 [arXiv:1811.06743] [INSPIRE].

[23] E. Budassi et al., *NNLO virtual and real leptonic corrections to muon-electron scattering*, *JHEP* **11** (2021) 098 [arXiv:2109.14606] [INSPIRE].

[24] D.R. Yennie, S.C. Frautschi and H. Suura, *The infrared divergence phenomena and high-energy processes*, *Annals Phys.* **13** (1961) 379 [INSPIRE].

JHEP01(2023)112

[25] E. Budassi, C.M. Carloni Calame, C.L. Del Pio and F. Piccinini, *Single π^0 production in μe scattering at MUonE*, *Phys. Lett. B* **829** (2022) 137138 [arXiv:2203.01639] [INSPIRE].

[26] P. Banerjee, T. Engel, A. Signer and Y. Ulrich, *QED at NNLO with McMule*, *SciPost Phys.* **9** (2020) 027 [arXiv:2007.01654] [INSPIRE].

[27] T. Engel, A. Signer and Y. Ulrich, *A subtraction scheme for massive QED*, *JHEP* **01** (2020) 085 [arXiv:1909.10244] [INSPIRE].

[28] S. Frixione, Z. Kunszt and A. Signer, *Three jet cross-sections to next-to-leading order*, *Nucl. Phys. B* **467** (1996) 399 [hep-ph/9512328] [INSPIRE].

[29] R. Frederix, S. Frixione, F. Maltoni and T. Stelzer, *Automation of next-to-leading order computations in QCD: the FKS subtraction*, *JHEP* **10** (2009) 003 [arXiv:0908.4272] [INSPIRE].

[30] R. Bonciani et al., *Two-loop four-fermion scattering amplitude in QED*, *Phys. Rev. Lett.* **128** (2022) 022002 [arXiv:2106.13179] [INSPIRE].

[31] M.K. Mandal, P. Mastrolia, J. Ronca and W.J. Bobadilla Torres, *Two-loop scattering amplitude for heavy-quark pair production through light-quark annihilation in QCD*, *JHEP* **09** (2022) 129 [arXiv:2204.03466] [INSPIRE].

[32] P. Mastrolia, M. Passera, A. Primo and U. Schubert, *Master integrals for the NNLO virtual corrections to μe scattering in QED: the planar graphs*, *JHEP* **11** (2017) 198 [arXiv:1709.07435] [INSPIRE].

[33] S. Di Vita, S. Laporta, P. Mastrolia, A. Primo and U. Schubert, *Master integrals for the NNLO virtual corrections to μe scattering in QED: the non-planar graphs*, *JHEP* **09** (2018) 016 [arXiv:1806.08241] [INSPIRE].

[34] A.A. Penin, *Two-loop photonic corrections to massive Bhabha scattering*, *Nucl. Phys. B* **734** (2006) 185 [hep-ph/0508127] [INSPIRE].

[35] A. Mitov and S. Moch, *The singular behavior of massive QCD amplitudes*, *JHEP* **05** (2007) 001 [hep-ph/0612149] [INSPIRE].

[36] T. Becher and K. Melnikov, *Two-loop QED corrections to Bhabha scattering*, *JHEP* **06** (2007) 084 [arXiv:0704.3582] [INSPIRE].

[37] T. Engel, C. Gnendiger, A. Signer and Y. Ulrich, *Small-mass effects in heavy-to-light form factors*, *JHEP* **02** (2019) 118 [arXiv:1811.06461] [INSPIRE].

[38] P. Banerjee, T. Engel, N. Schalch, A. Signer and Y. Ulrich, *Bhabha scattering at NNLO with next-to-soft stabilisation*, *Phys. Lett. B* **820** (2021) 136547 [arXiv:2106.07469] [INSPIRE].

[39] F. Buccioni, S. Pozzorini and M. Zoller, *On-the-fly reduction of open loops*, *Eur. Phys. J. C* **78** (2018) 70 [arXiv:1710.11452] [INSPIRE].

[40] F. Buccioni et al., *OpenLoops* 2, *Eur. Phys. J. C* **79** (2019) 866 [arXiv:1907.13071] [INSPIRE].

[41] T. Engel, A. Signer and Y. Ulrich, *Universal structure of radiative QED amplitudes at one loop*, *JHEP* **04** (2022) 097 [arXiv:2112.07570] [INSPIRE].

[42] F.E. Low, *Bremsstrahlung of very low-energy quanta in elementary particle collisions*, *Phys. Rev.* **110** (1958) 974 [INSPIRE].

[43] T.H. Burnett and N.M. Kroll, *Extension of the low soft photon theorem*, *Phys. Rev. Lett.* **20** (1968) 86 [INSPIRE].

JHEP01(2023)112

[44] S. Kollatzsch and Y. Ulrich, *Lepton pair production at NNLO in QED with EW effects*, arXiv:2210.17172 [INSPIRE].

[45] A. Nikishov, *Radiative corrections to the scattering of μ mesons on electrons*, *Sov. Phys. JETP* **12** (1961) 529.

[46] K.E. Eriksson, *Radiative corrections to muon-electron scattering*, *Nuovo Cim.* **19** (1961) 1029.

[47] K.E. Eriksson, B. Larsson and G.A. Rinander, *Radiative corrections to muon-electron scattering*, *Nuovo Cim.* **30** (1963) 1434.

[48] P. Van Nieuwenhuizen, *Muon-electron scattering cross-section to order α^3*, *Nucl. Phys. B* **28** (1971) 429 [INSPIRE].

[49] T.V. Kukhto, N.M. Shumeiko and S.I. Timoshin, *Radiative corrections in polarized electron muon elastic scattering*, *J. Phys. G* **13** (1987) 725 [INSPIRE].

[50] D.Y. Bardin and L. Kalinovskaya, *QED corrections for polarized elastic μe scattering*, hep-ph/9712310 [INSPIRE].

[51] N. Kaiser, *Radiative corrections to lepton-lepton scattering revisited*, *J. Phys. G* **37** (2010) 115005 [INSPIRE].

[52] C. Gnendiger et al., *To d, or not to d: recent developments and comparisons of regularization schemes*, *Eur. Phys. J. C* **77** (2017) 471 [arXiv:1705.01827] [INSPIRE].

[53] P. Mastrolia and E. Remiddi, *Two loop form-factors in QED*, *Nucl. Phys. B* **664** (2003) 341 [hep-ph/0302162] [INSPIRE].

[54] R. Bonciani, P. Mastrolia and E. Remiddi, *QED vertex form-factors at two loops*, *Nucl. Phys. B* **676** (2004) 399 [hep-ph/0307295] [INSPIRE].

[55] W. Bernreuther et al., *Two-loop QCD corrections to the heavy quark form-factors: the vector contributions*, *Nucl. Phys. B* **706** (2005) 245 [hep-ph/0406046] [INSPIRE].

[56] P. Banerjee, T. Engel, N. Schalch, A. Signer and Y. Ulrich, *Møller scattering at NNLO*, *Phys. Rev. D* **105** (2022) L031904 [arXiv:2107.12311] [INSPIRE].

[57] T. Engel, *Muon-electron scattering at NNLO*, Ph.D. thesis, Universität Zürich, Zürich, Switzerland (2022) [arXiv:2209.11110] [INSPIRE].

[58] A. Denner, S. Dittmaier and L. Hofer, *Collier: a fortran-based Complex One-Loop LIbrary in Extended Regularizations*, *Comput. Phys. Commun.* **212** (2017) 220 [arXiv:1604.06792] [INSPIRE].

[59] A. van Hameren, *OneLOop: for the evaluation of one-loop scalar functions*, *Comput. Phys. Commun.* **182** (2011) 2427 [arXiv:1007.4716] [INSPIRE].

[60] M.J. Levine and R. Roskies, *Hyperspherical approach to quantum electrodynamics — sixth-order magnetic moment*, *Phys. Rev. D* **9** (1974) 421 [INSPIRE].

[61] M.J. Levine, R.C. Perisho and R. Roskies, *Analytic contributions to the G factor of the electron*, *Phys. Rev. D* **13** (1976) 997 [INSPIRE].

[62] S. Laporta, *Hyperspherical integration and the triple cross vertex graphs*, *Nuovo Cim. A* **107** (1994) 1729 [hep-ph/9404203] [INSPIRE].

[63] A. Djouadi and P. Gambino, *Electroweak gauge bosons selfenergies: complete QCD corrections*, *Phys. Rev. D* **49** (1994) 3499 [hep-ph/9309298] [INSPIRE].

JHEP01(2023)112

[64] F. Jegerlehner, *Software packages alphaQED and pQCDAdler*, http://www-com.physik.hu-berlin.de/~fjeger/software.html.

[65] T. Hahn, *Generating Feynman diagrams and amplitudes with FeynArts* 3, *Comput. Phys. Commun.* **140** (2001) 418 [hep-ph/0012260] [INSPIRE].

[66] V. Shtabovenko, R. Mertig and F. Orellana, *New developments in FeynCalc* 9.0, *Comput. Phys. Commun.* **207** (2016) 432 [arXiv:1601.01167] [INSPIRE].

[67] P. Mastrolia, T. Peraro, A. Primo, J. Ronca and W.J. Torres Bobadilla, *AIDA, Adaptive Integrand Decomposition Algorithm.*

[68] P. Mastrolia, T. Peraro and A. Primo, *Adaptive Integrand Decomposition in parallel and orthogonal space*, *JHEP* **08** (2016) 164 [arXiv:1605.03157] [INSPIRE].

[69] P. Mastrolia, A. Primo and W.J. Torres Bobadilla, *Multi-gluon scattering amplitudes at one-loop and color-kinematics duality*, in preparation (2016).

[70] A. von Manteuffel and C. Studerus, *Reduze* 2 — *distributed Feynman integral reduction*, arXiv:1201.4330 [INSPIRE].

[71] G. Barucchi and G. Ponzano, *Differential equations for one-loop generalized feynman integrals*, *J. Math. Phys.* **14** (1973) 396 [INSPIRE].

[72] A.V. Kotikov, *Differential equations method: new technique for massive Feynman diagrams calculation*, *Phys. Lett. B* **254** (1991) 158 [INSPIRE].

[73] E. Remiddi, *Differential equations for Feynman graph amplitudes*, *Nuovo Cim. A* **110** (1997) 1435 [hep-th/9711188] [INSPIRE].

[74] T. Gehrmann and E. Remiddi, *Differential equations for two loop four point functions*, *Nucl. Phys. B* **580** (2000) 485 [hep-ph/9912329] [INSPIRE].

[75] J.M. Henn, *Multiloop integrals in dimensional regularization made simple*, *Phys. Rev. Lett.* **110** (2013) 251601 [arXiv:1304.1806] [INSPIRE].

[76] M. Argeri et al., *Magnus and Dyson series for master integrals*, *JHEP* **03** (2014) 082 [arXiv:1401.2979] [INSPIRE].

[77] S. Di Vita, P. Mastrolia, U. Schubert and V. Yundin, *Three-loop master integrals for ladder-box diagrams with one massive leg*, *JHEP* **09** (2014) 148 [arXiv:1408.3107] [INSPIRE].

[78] A.B. Goncharov, *Multiple polylogarithms, cyclotomy and modular complexes*, *Math. Res. Lett.* **5** (1998) 497 [arXiv:1105.2076] [INSPIRE].

[79] T. Gehrmann and E. Remiddi, *Numerical evaluation of two-dimensional harmonic polylogarithms*, *Comput. Phys. Commun.* **144** (2002) 200 [hep-ph/0111255] [INSPIRE].

[80] M. Czakon, *Tops from light quarks: full mass dependence at two-loops in QCD*, *Phys. Lett. B* **664** (2008) 307 [arXiv:0803.1400] [INSPIRE].

[81] R. Bonciani, A. Ferroglia, T. Gehrmann, D. Maitre and C. Studerus, *Two-loop fermionic corrections to heavy-quark pair production: the quark-antiquark channel*, *JHEP* **07** (2008) 129 [arXiv:0806.2301] [INSPIRE].

[82] R. Bonciani, A. Ferroglia, T. Gehrmann and C. Studerus, *Two-loop planar corrections to heavy-quark pair production in the quark-antiquark channel*, *JHEP* **08** (2009) 067 [arXiv:0906.3671] [INSPIRE].

JHEP01(2023)112

[83] P. Nogueira, *Automatic Feynman graph generation*, *J. Comput. Phys.* **105** (1993) 279 [INSPIRE].

[84] H.H. Patel, *Package-X: a Mathematica package for the analytic calculation of one-loop integrals*, *Comput. Phys. Commun.* **197** (2015) 276 [arXiv:1503.01469] [INSPIRE].

[85] T. Becher and M. Neubert, *Infrared singularities of QCD amplitudes with massive partons*, *Phys. Rev. D* **79** (2009) 125004 [arXiv:0904.1021] [INSPIRE].

[86] T. Becher and M. Neubert, *On the structure of infrared singularities of gauge-theory amplitudes*, *JHEP* **06** (2009) 081 [arXiv:0903.1126] [INSPIRE].

[87] R.J. Hill, *Effective field theory for large logarithms in radiative corrections to electron proton scattering*, *Phys. Rev. D* **95** (2017) 013001 [arXiv:1605.02613] [INSPIRE].

[88] A. Broggio, C. Gnendiger, A. Signer, D. Stöckinger and A. Visconti, *SCET approach to regularization-scheme dependence of QCD amplitudes*, *JHEP* **01** (2016) 078 [arXiv:1506.05301] [INSPIRE].

[89] C. Gnendiger, A. Signer and A. Visconti, *Regularization-scheme dependence of QCD amplitudes in the massive case*, *JHEP* **10** (2016) 034 [arXiv:1607.08241] [INSPIRE].

[90] W.B. Kilgore, *The four dimensional helicity scheme beyond one loop*, *Phys. Rev. D* **86** (2012) 014019 [arXiv:1205.4015] [INSPIRE].

[91] C. Gnendiger, A. Signer and D. Stöckinger, *The infrared structure of QCD amplitudes and $H \to gg$ in FDH and DRED*, *Phys. Lett. B* **733** (2014) 296 [arXiv:1404.2171] [INSPIRE].

[92] Y. Ulrich, *McMule — QED corrections for low-energy experiments*, Ph.D. thesis, Universität Zürich, Zürich, Switzerland (2020) [arXiv:2008.09383] [INSPIRE].

[93] C.W. Bauer, S. Fleming, D. Pirjol and I.W. Stewart, *An effective field theory for collinear and soft gluons: heavy to light decays*, *Phys. Rev. D* **63** (2001) 114020 [hep-ph/0011336] [INSPIRE].

[94] C.W. Bauer, D. Pirjol and I.W. Stewart, *Soft collinear factorization in effective field theory*, *Phys. Rev. D* **65** (2002) 054022 [hep-ph/0109045] [INSPIRE].

[95] M. Beneke, A.P. Chapovsky, M. Diehl and T. Feldmann, *Soft collinear effective theory and heavy to light currents beyond leading power*, *Nucl. Phys. B* **643** (2002) 431 [hep-ph/0206152] [INSPIRE].

[96] M. Beneke and V.A. Smirnov, *Asymptotic expansion of Feynman integrals near threshold*, *Nucl. Phys. B* **522** (1998) 321 [hep-ph/9711391] [INSPIRE].

[97] McMule team, *Gitlab webpage*, https://mule-tools.gitlab.io/.

[98] L. Naterop, A. Signer and Y. Ulrich, *handyG — rapid numerical evaluation of generalised polylogarithms in fortran*, *Comput. Phys. Commun.* **253** (2020) 107165 [arXiv:1909.01656] [INSPIRE].

[99] Y. Ulrich et al., McMule *dataset*, Zenodo (2022).

[100] L. Lannelongue, J. Grealey and M. Inouye, *Green algorithms: quantifying the carbon footprint of computation*, *Adv. Sci.* **8** (2021) 2100707.

[101] Particle Data Group collaboration, *Review of particle physics*, *PTEP* **2022** (2022) 083C01 [INSPIRE].

JHEP01(2023)112

[102] Z. Bern, L.J. Dixon and A. Ghinculov, *Two loop correction to Bhabha scattering*, *Phys. Rev. D* **63** (2001) 053007 [hep-ph/0010075] [INSPIRE].

[103] M. Fael, F. Lange, K. Schönwald and M. Steinhauser, *Singlet and nonsinglet three-loop massive form factors*, *Phys. Rev. D* **106** (2022) 034029 [arXiv:2207.00027] [INSPIRE].

[104] M. Fael, F. Lange, K. Schönwald and M. Steinhauser, *Massive vector form factors to three loops*, *Phys. Rev. Lett.* **128** (2022) 172003 [arXiv:2202.05276] [INSPIRE].

[105] L.W. Garland, T. Gehrmann, E.W.N. Glover, A. Koukoutsakis and E. Remiddi, *The two loop QCD matrix element for* $e^+e^- \to 3$ *jets*, *Nucl. Phys. B* **627** (2002) 107 [hep-ph/0112081] [INSPIRE].

[106] L.W. Garland, T. Gehrmann, E.W.N. Glover, A. Koukoutsakis and E. Remiddi, *Two loop QCD helicity amplitudes for* $e^+e^- \to 3$ *jets*, *Nucl. Phys. B* **642** (2002) 227 [hep-ph/0206067] [INSPIRE].

[107] M. Hidding, *DiffExp, a Mathematica package for computing Feynman integrals in terms of one-dimensional series expansions*, *Comput. Phys. Commun.* **269** (2021) 108125 [arXiv:2006.05510] [INSPIRE].

[108] X. Liu and Y.-Q. Ma, *AMFlow: a Mathematica package for Feynman integrals computation via auxiliary mass flow*, *Comput. Phys. Commun.* **283** (2023) 108565 [arXiv:2201.11669] [INSPIRE].

[109] S. Borowka, G. Heinrich, S.P. Jones, M. Kerner, J. Schlenk and T. Zirke, *SecDec-3.0: numerical evaluation of multi-scale integrals beyond one loop*, *Comput. Phys. Commun.* **196** (2015) 470 [arXiv:1502.06595] [INSPIRE].

[110] Y. Ulrich, *N^3LO kick-off workstop/thinkstart*, https://conference.ippp.dur.ac.uk/event/1104/, Durham, U.K., 3–5 August 2022.

[111] M. Heller, *Planar two-loop integrals for μe scattering in QED with finite lepton masses*, arXiv:2105.08046 [INSPIRE].

JHEP01(2023)112